AD-A154 044 MEASUREMENTS OF FOLDED PATH OPTICAL SCINTILLATION USING A CORNER CUBE A CAT'S EYE AND A FLAT MIRROR REFLECTOR (U) NAVAL POSTGRADUATE SCHOOL MONTEREY CA J H KIM 1/1

UNCLASSIFIED DEC 84 F/G 20/6 NL

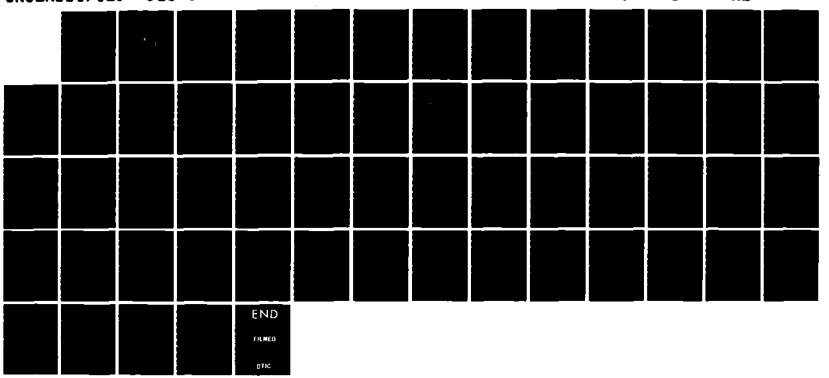

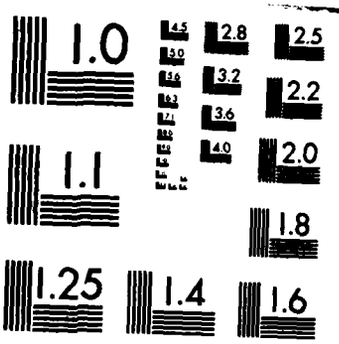

(2)

NAVAL POSTGRADUATE SCHOOL

Monterey, California

THESIS

MEASUREMENTS OF FOLDED PATH OPTICAL SCINTILLATION USING A CORNER CUBE, A CAT'S EYE AND A FLAT MIRROR REFLECTOR

by

Jong Hwan Kim

December 1984

Thesis Advisor: E. A. Milne

Approved for public release; distribution is unlimited.

SECURITY CLASSIFICATION OF THIS PAGE (When Data Entered)

REPORT DOCUMENTATION PAGE		READ INSTRUCTIONS BEFORE COMPLETING FORM
1. REPORT NUMBER	2. GOVT ACCESSION NO.	3. RECIPIENT'S CATALOG NUMBER
4. TITLE (and Subtitle) Measurements of Folded Path Optical Scintillation Using a Corner Cube, A Cat's Eye and a Flat Mirror Reflector		5. TYPE OF REPORT & PERIOD COVERED Master's Thesis; December 1984 6. PERFORMING ORG. REPORT NUMBER
7. AUTHOR(s) Jong Hwan Kim		8. CONTRACT OR GRANT NUMBER(s)
9. PERFORMING ORGANIZATION NAME AND ADDRESS Naval Postgraduate School Monterey, California 93943		10. PROGRAM ELEMENT, PROJECT, TASK AREA & WORK UNIT NUMBERS
11. CONTROLLING OFFICE NAME AND ADDRESS Naval Postgraduate School Monterey, California 93943		12. REPORT DATE December 1984 13. NUMBER OF PAGES 57
14. MONITORING AGENCY NAME & ADDRESS(if different from Controlling Office)		15. SECURITY CLASS. (of this report) 15a. DECLASSIFICATION/ DOWNGRADING SCHEDULE

16. DISTRIBUTION STATEMENT (of this Report)

Approved for public release; distribution is unlimited.

17. DISTRIBUTION STATEMENT (of the abstract entered in Block 20, if different from Report)

18. SUPPLEMENTARY NOTES

19. KEY WORDS (Continue on reverse side if necessary and identify by block number)

Scintillation, Path, Weighting

20. ABSTRACT (Continue on reverse side if necessary and identify by block number)

A theoretical prediction of the folded path weighting function for optical scintillation strength was made by Dr. Avinu Ze'evi. In an effort to verify this prediction, a sixty-one meter, enclosed turbulence chamber was built, allowing the position of a turbulence source to be moved and the scintillation strength measured at different path positions. This experiment tested the Ze'evi hypothesis using a corner cube, a cat's eye and a flat mirror and compared the results of each. The experimental results do not follow Dr. Ze'evi's theory. The general pattern of both the corner cube

DD FORM 1 JAN 73 1473 EDITION OF 1 NOV 65 IS OBSOLETE
S/N 0102-LF-014-6601

SECURITY CLASSIFICATION OF THIS PAGE (When Data Entered)

and the flat mirror have less weight at the target end than predicted. The cat's eye scintillation followed the predicted weighting.

(Keywords include:)

(19)

Approved for public release; distribution is unlimited.

Measurements of Folded Path Optical Scintillation Using a Corner Cube, a Cat's Eye and a Flat Mirror Reflector

by

Jong Hwan Kim
Lcdr, Republic of Korea Navy
B.S., Korea Naval Academy, 1973
B.S., Seoul National University, 1977

Submitted in partial fulfillment of the requirements for the degree of

MASTER OF SCIENCE IN PHYSICS

from the

NAVAL POSTGRADUATE SCHOOL
December 1984

Author: Kim Jong Hwan
Jong Hwan Kim

Approved by: Edmund A Milne
E. A. Milne, Thesis Advisor

Donald L Walters
D. L. Walters, Second Reader

G E Schacher
G. E. Schacher, Chairman,
Department of Physics

J N Dyer
J. N. Dyer,
Dean of Science and Engineering

ABSTRACT

A theoretical prediction of the folded path weighting function for optical scintillation strength was made by Dr. Avihu Ze'evi. In an effort to verify this prediction, a sixty - one meter, enclosed turbulence chamber was built, allowing the position of a turbulence source to be moved and the scintillation strength measured at different path positions. This experiment tested the Ze'evi hypothesis using a corner cube, a cat's eye and a flat mirror and compared the results of each. The experimental results do not follow Dr. Ze'evi's theory. The general pattern of both the corner cube and the flat mirror have less weight at the detector end than predicted and more weight at the target end than predicted. The cat's eye scintillation followed the predicted weighting.

TABLE OF CONTENTS

LIST OF FIGURES

ACKNOWLEDGMENTS

I wish to thank the assistance of B. G. An and J. B. Lee without whose help the completion of this project would not have been possible. I would also like to thank professor D. L. Walters for his aid with the theory of the turbulence chamber. Finally, a special note of thanks is given to professor E. A. Milne who freely give of his time to instruct the author in experimental procedures and analysis of data, ever present guidance and direction.

I. INTRODUCTION

A. GENERAL

In optical propagation through a turbulent atmosphere, fluctuations in the atmospheric refractive index causes random deviations in phase across the propagation wavefront. Familiar examples are the twinkling of stars or the image boil of lasers, a form of scintillation. Scintillation results from random fluctuations of the index of refraction of the atmosphere causing constructive and destructive interference (wave front tilt and loss of resolution). These interference effects are recognized by an observer as changes in irradiance, or intensity of the incident beam radiation.

B. THEORY

The theory of the random fluctuations of the refractive index produced in a weak turbulence region was developed by Tatarski [Ref. 1] and uses the normalized log amplitude variance given by:

$$\chi^2 = B_\chi(0) = 2\pi \iint Fx(K) K\, dK,$$

$$= 2\pi \int K\, dK \int 2\pi k^2 \Phi(z) \sin^2\left[K^2(L-z)/2k\right] dz,$$

$$= 0.307\, C_n^2\, k^{7/6} L^{11/6} \quad \text{(plane wave)} \quad (1.1)$$

$$= 0.124\, C_n^2\, k^{7/6} L^{11/6} \quad \text{(spherical wave)} \quad (1.2)$$

where $k = 2\pi/\lambda$

λ ; optical wavelength

L ; path length from source to detector

C ; refractive index structure constant

The plane wave expression is valid for a point receiver. The spherical wave expression is varied for a point source and point receiver.

Under appropriate conditions, scintillation can be measured by placing a detector in the observation plane and recording the intensity changes over time of the radiation. The intensity fluctuations are computed, rigorously, by calculating the variance of the intensity, i.e.

$$\begin{aligned}\sigma_{I/I_0}^2 &= \langle (I/I_0)^2 \rangle - \langle I/I_0 \rangle^2 \\ &= \left[\langle I^2 \rangle - \langle I \rangle^2 \right] / I_0^2 \\ &= \sigma_I^2 / I_0^2 \end{aligned} \qquad (1.3)$$

where $I = I(r,t)$; the instantaneous intensity at the detector.

$I = \langle I(r,t) \rangle$; the ensemble average.

$\sigma_I^2 = \langle I^2 \rangle - \langle I \rangle^2$; the varance.

Tatarski [Ref. 1] showed that, for the weak trubulence region, the log irradiance fluctuations have a Gaussian distribution. The log intensity variance is determined as follows:

$$\begin{aligned} \chi &= \log (I/I_0) \\ \sigma_\chi^2 &= \langle \chi^2 \rangle - \langle \chi \rangle^2 \\ \sigma_\chi^2 &= \langle (\log I/I_0)^2 \rangle - \langle \log I/I_0 \rangle^2 \\ &= \langle (\log I)^2 \rangle - \langle \log I \rangle^2 \\ \sigma_\chi^2 &= \sigma^2(\log I) \end{aligned} \qquad (1.4)$$

The log intensity variance σ_χ^2 is of importance in describing the distribution of turbulence. This allows the scintillation to be described by the variance of log intensity fluctuations received at a detector with no dependence on the average signal intensity received. Clifford noted [Ref. 10] that the relationship $\sigma_\chi^2 = 4\sigma_K^2$ is the accepted formula to correlate the empirical (σ_χ^2) and the theoretical

(σ_K^2) variances. This results in our being able to describe the scintillation for spherical waves in the low turbulence region by:

$$\sigma_l^2 = 4\,\sigma_K^2 = 4A\,C_n^2\,K^{7/6}L^{11/6} \qquad (1.5)$$

where $\sigma^2 \leq 1$;defines the low turbulence region.

Tatarski showed that this relation is valid only in a weak, homogeneous turbulence of the Kolmogorov form. A crucial assumption in this and in preceding works by Speer, B. A. and Parker, F. H. [Ref. 5] Costantine, A. G. [Ref. 7] and Henry, L. M. [Ref. 8] is that we satisfy this condition.

If the turbulence is not constant along the propagation path, there must be some weighting for position. The works of Tatarski [Ref. 1] Lutomirski and Yura [Ref. 3] and others had explained the direct path scintillation clearly with the theory in reasonable agreement with experiment. But the folded path scintillation case is not as well understood, and theoretical predictions have not been fully confirmed by experiment.

Optical scintillation on folded paths was investigated by Dr. Avihu Ze'evi in his doctorial thesis at NPGS. In his work, Dr. Ze'evi examined spherical waves and a plane mirror a folding target, and weak, Kolmogorov turbulence. Z. e. stated that the relative contribution to the scintillation of different points along the path of a spherical wave are:

$$\text{direct path} : W(x) = [x(1-x)]^{5/6} \qquad (1.6)$$

$$\text{folded path} : W(x) = [x(2-x)]^{5/6}, \qquad (1.7)$$

where $x = Z/Zo$

z ;distance along the path from the detector

z_o ;distance between detector and mirror,

III. EXPERIMENTAL WORK

A. EXPERIMENTAL GOALS

We had two main goals for our experiment. First, we wanted to get additional data to prove or disprove the theoretical folded path scintillation weighting function predicted by Ze'evi. Second, we wanted to use three different reflectors, a flat mirror, a corner cube and a cat's eye to compare our experimental results with each order.

B. PROCEDURE

The experimental data were taken at night. We assembled the tunnel sections on the roof of Spanagel Hall and sealed them together with masking tape to prevent unwanted drafts in the tunnel. The detector, the laser source, the chopper and all the reflectors were also sealed under the table protecting the ends of the tunnel, so that we had a closed system. The only openings were on the sides of the turbulence section, which allowed the flow of air into the region directly under the heater. Warmer air would then rise up the chimney.

Additionally, we observed an interference pattern on the detector face. This interference pattern was eliminated by intercepting the secondary beam from the back face of the beam splitter with a small wooden stick. Examination of the beam structure at the target mirror and on the detector face indicated that this eliminated the interference problem without introducting stucture to the beam.

Our research consisted of nine separate experiments. We do not include results of the first two experiments, because

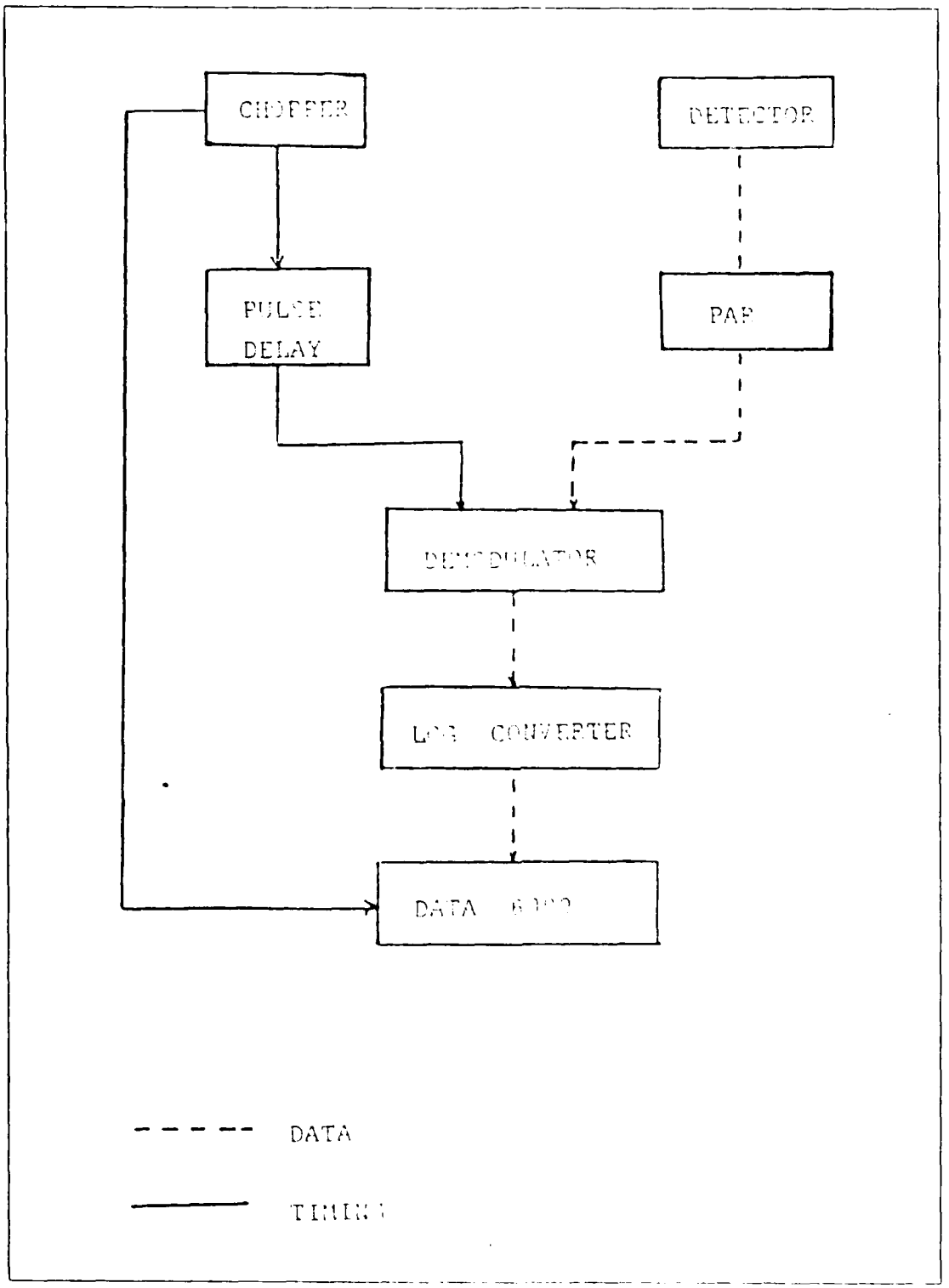

Figure 2.6 Block Diagram of Timing and Data Signals.

LED source and detector provided the basis for all timing within the system. The signal from the LED triggered a function generator, which provided the actual pulses for system timing.

E. DATA COLLECTION EQUIPMENT

The signals were detected by a silicon avalanche photodiode, then amplified by a Princeton Applied research model 113 amplifier with the gain set at 50. The high and low frequency roll-offs for the amplifier were carefully adjusted to get a properly amplified signal without creating spectral distortions. The amplifier output signal was sent directly to the demodulator, built at NPGS.

A trigger pulse activated the demodulator to demodulate the input signal. The demodulator utilized a sample and hold circuit to sample the instantaneous maximum and the background. The output of the demodulator was the difference between the two signals. This means that the true signal intensity was available for further processing. The result was passed to a log converter.

F. DATA REDUCTION EQUIPMENT

Finally, this signal which is now propotional to the log of the intensity was fed to the DATA 6000. This device took the log intensity fluctuations and calculated the standard deviation. Five sets of data, 500 samples each, were taken for each reflector, and 10 turbulence positions during an experimental run. These results were transferred to the Hewlett Packard model 9825B calculator for output to the plotter and printer.

Figure 2.6 gives a schematic layout of the pulse forming and detection equipment plus the respective signal processing and data reduction equipment.

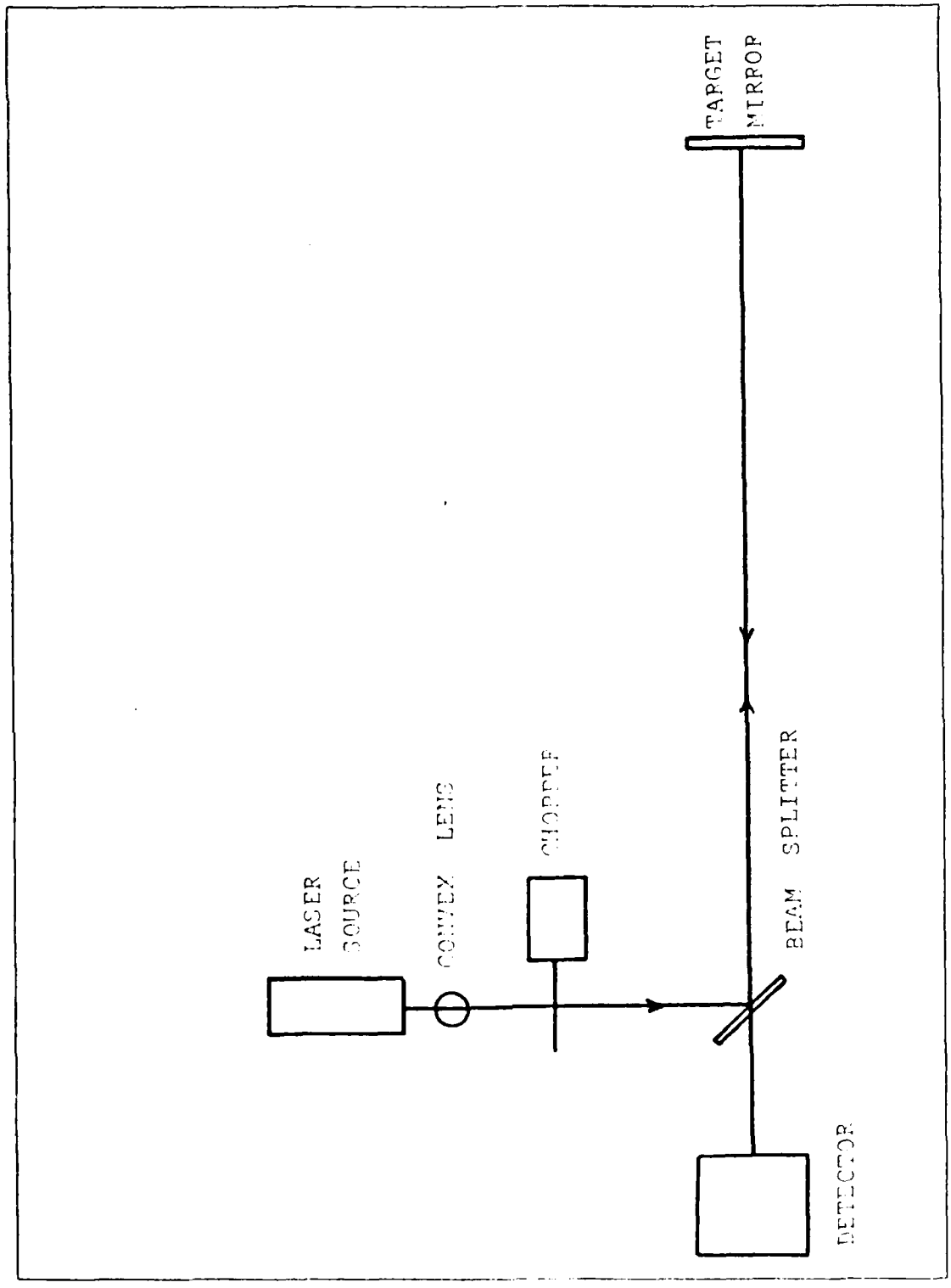

Figure 2.5 Arrangement of Optical Equipment.

C. OPTICS

We did not measure the direct path because Costantine [Ref. 7] and Henry [Ref. 8] have already made the measurements and their results agreed with theory. So that, we measured only the folded path beam. We set up a convex lens just in front of the laser source to diverge the beam. The beam was chopped by a mechanical chopper. The chopper modulated the signal for A.C. amplification. A beam splitter directed the beam towards the reflector located at the other end of the tunnel. In our experiment, we concentrated on the flat mirror, corner cube, and cat's eye to compare the results with each other.

At first, by placing the corner cube and cat's eye on an optical bench, we hoped that we could slide the corner cube and cat's eye into the beam, without disturbing the alignment of the flat mirror. But we were unable to insert the corner cube or cat's eye without disturbing the alignment of the mirror. So we completed all measurements for the corner cube then we made the measurements with the flat mirror and finally the cat's eye. The arrangement of the optical components is shown in Figure 2.5.

D. LASER SOURCES AND PULSE FORMING EQUIPMENT

The laser used for the experiment was a HeNe laser with a wavelength 0.6328 micrometers and power output of 0.95 milliwatts. The laser was mounted on a platform controlled by micrometer screw adjustments to facilitate precision alignment.

The mechanical chopper with an open to closed ratio of 1 : 4 was mounted just in front of the laser source. In order to establish a trigger pulse synchronous with the optical pulse, a light emitting diode was positioned on the opposite side of the chopper wheel from a detector. The pulse from a

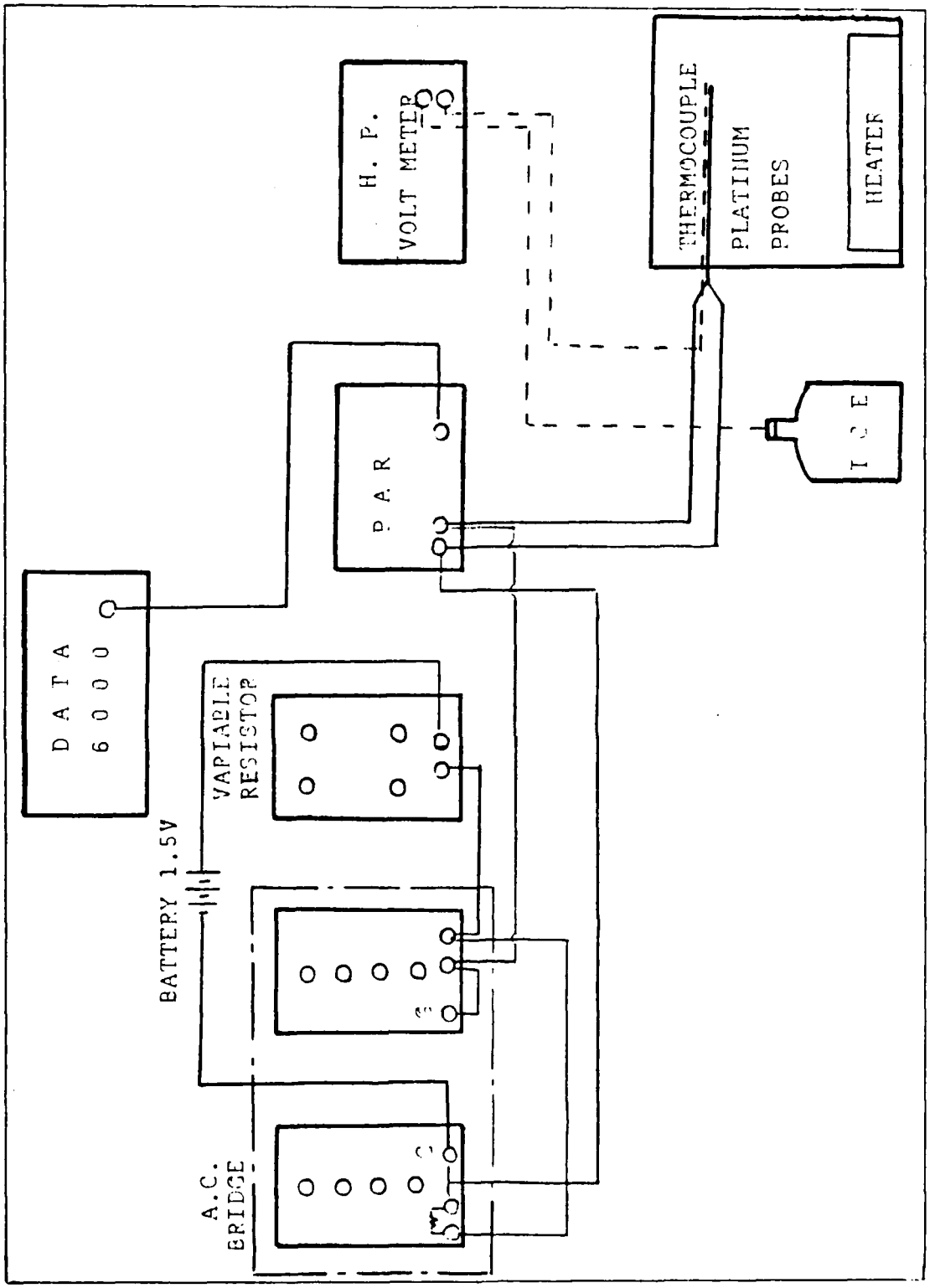

Figure 2.4 Schematic of C_T^2 system.

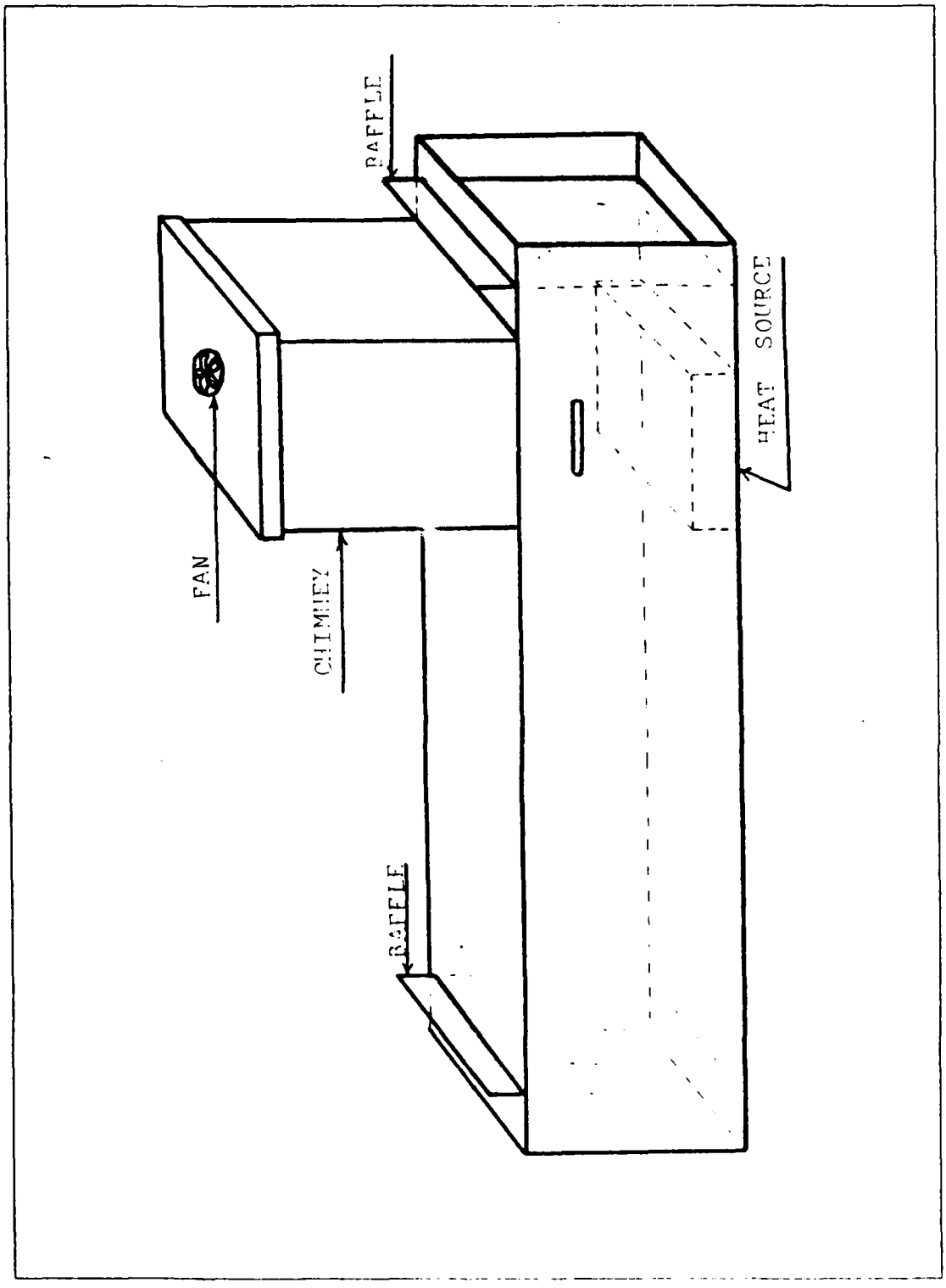

Figure 2.3 Turbulence Chamber.

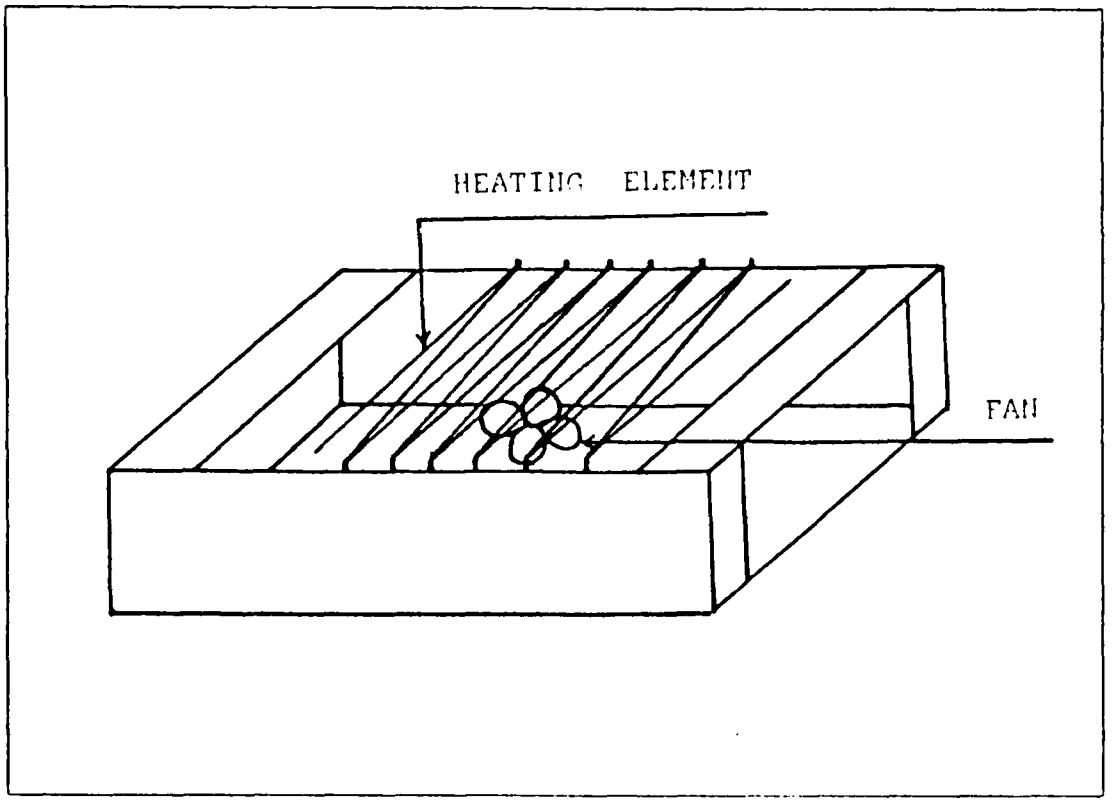

Figure 2.2 Heat Source.

involved in the experiment. In order to have the same quantitative measure of the turbulence present, the temperature structure constant, C_T^2 was measured at each path position of the modified tunnel section during an experimental run. C_T^2 was measured by inserting 2 platinum resistance probes and a thermocouple directly above the heat source screen. Five such runs were made and averaged at each heat source location at the same time scintillation data were collected. A schematic of the system is shown in Figure 2.4. Details of this procedure can be found in [Ref. 6].

A chimney 64 cm square x 64 cm high was constructed over the opening. A wooden baffle was placed over the top of the chimney so as to allow air flow but prevent down drafts from entering the tunnel. We installed a fan in the baffle in the top of the chimney, directed so that it exhausted air from the heater section to the outside. In addition, two plywood baffles were installed inside the chamber next to the heater. These baffles limited the flow of air along the longitudinal axis of the tunnel. Elliptical holes of sufficient size were cut in the baffles to allow the beam to pass through without any additional diffration effects.

A wide slit was cut in the side just below the heater. This allowed air to flow in under the heater where it was drawn up through the heater by convection.

A small slit was cut in the side of the turbulence section just above the optical path. This was for inserting the platinum temperature probes above the heat source for measuring the temperature fluctuations.

The heating element was bent in reversing V's mounted on a wooden stand with ceramic stand offs. The wide spacings, about 6 centimeters, between the legs of the V's helped in providing a larger outer scale. A fan turning slowly at about 1 revolution per second helped break up the laminar flow above the heater into turbulent flow as close to the heater as possible. The detailed statistics are presented in [Ref. 9].

The turbulence source was mounted in a special tunnel section. This unit could replace any tunnel section during an experiment. Figures 2.2 and 2.3 show the heater sections and turbulence chamber.

For our experiment the turbulence source was introduced at different positions along the path. This change of turbulence location could be completed in several minutes without disturbing or adjusting any optical components

is on the order of meters, Then the Equation 2.3 is valid. For some larger r, the temperature fluctuations become uncorrelated and the structure function asymptotically approaches a limit. Squaring the quantity in brackets in Equation 2.2, we have

$$D_T(r) = \langle T(r_2)^2 + T(r_1)^2 - 2T(r_2)T(r_1)\rangle \qquad (2.5)$$

For r -- , and assuming homogeneity, $\langle T(r_1)\rangle = \langle T(r_2)\rangle$, the structure function becomes

$$D_T(r) = 2\left[\langle T^2(r_1)\rangle - \langle T(r_1)\rangle^2\right]$$
$$= 2\sigma_T^2 . \qquad (2.6)$$

Equation 2.6 shows that the asymptotic limit of $D_T(r)$ is just twice the variance of the temperature.

According to the above theory, we found that a reasonable value of the distance between the two probes (r) was 0.05m. One sample experiment of the variation of D_T with r is located in Appendix K.

A tunnel 61 meters long with a cross section of 0.61 meter x 0.61 meter was constructed by Costantine [Ref. 7] and Flenniken [Ref. 6]. They used four pieces of 3/8 inch plywood 2 feet by 8 feet to construct a section of tunnel. The tunnel consisted of 25 sections placed end to end. The plywood was treated with a water repellant and painted white on the outside and flat black on the inside. The tunnel was located on the roof of Spanegal Hall. The plywood sections were sealed together by prevent any drafts inside the tunnel.

One section was modified for the controlled turbulence region. A heat source was placed just above the bottom at one end of the section and an opening about the same size as the area of the heat source was cut in the top just above the heat source.

By dimensional analysis, Kolmogorov showed that as long as r was restricted to a certain interval called the inertial subrange, then equation (2.2) had a simple $r^{2/3}$ power law dependence

$$D_T(r) = C_T^2 r^{2/3} \qquad (2.3)$$

and the index of refraction structure function is

$$D_n(r) = C_n^2 r^{2/3} = C_T^2 r^{4/3} (79\ P/T^2 \times 10^{-6})^2 \qquad (2.4)$$

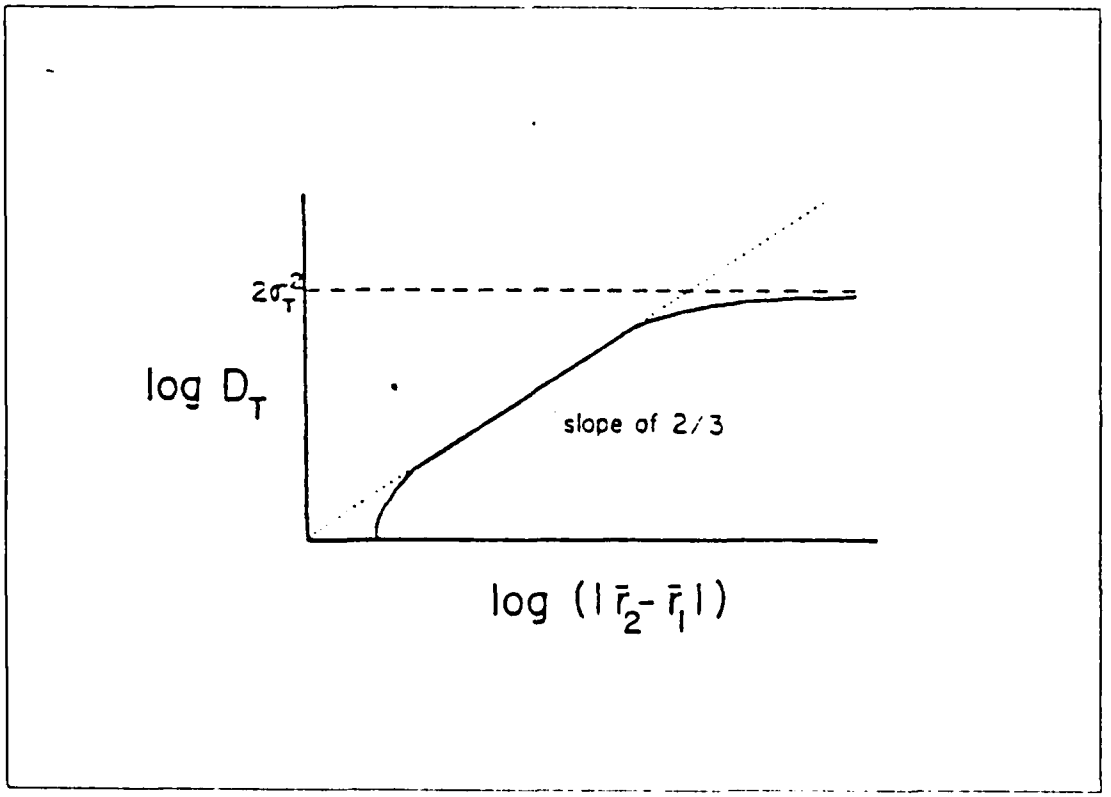

Figure 2.1 Log D_T vs Log$(|r_2 - r_1|)$.

The variation of $D_T = f(r)$ is shown in Figure (2.1). As long as r is greater than the inner-scale, which is on the order of millimeters, and smaller than an outer-scale, which

II. EXPERIMENTAL APPROACH

A. GENERAL CONSIDERATIONS

As a result of previous work at NPS on the effects of the turbulent atmosphere on optical propagation and the attempts by others to validate portions of Ze'evi's doctoral thesis, most of the optical and processing equipment required for this experiment was already in existence. We made only minor modifications of the turbulence chamber used to cause scintillation along the path. The turbulence needed to be as reproducible as possible. C_T^2 was measured at each position in order to normalize our results. We briefly describe the compomemts of the scintillation measuring system in the following section.

B. TURBULENCE CHAMBER

Tatarski [Ref. 1] defined the structure functions for temperature as

$$D_T(r_2 - r_1) = \langle [T(r_2) - T(r_1)]^2 \rangle \qquad (2.1)$$

This is the general form for a structure function and can be used for other variables such as wind speed, humidity, and aerosol concentration. The brackets < > imply an ensemble average in which all possible point pairs r_2, r_1 are averaged. By imposing isotropy, we remove the dependence on the vector coordinates and only need to consider the magnitude $r = |\bar{r}_2 - \bar{r}_1|$ of the difference between the two points. The temperature structure function becomes

$$D_T(r) = \langle [T(r_2) - T(r_1)]^2 \rangle \qquad (2.2)$$

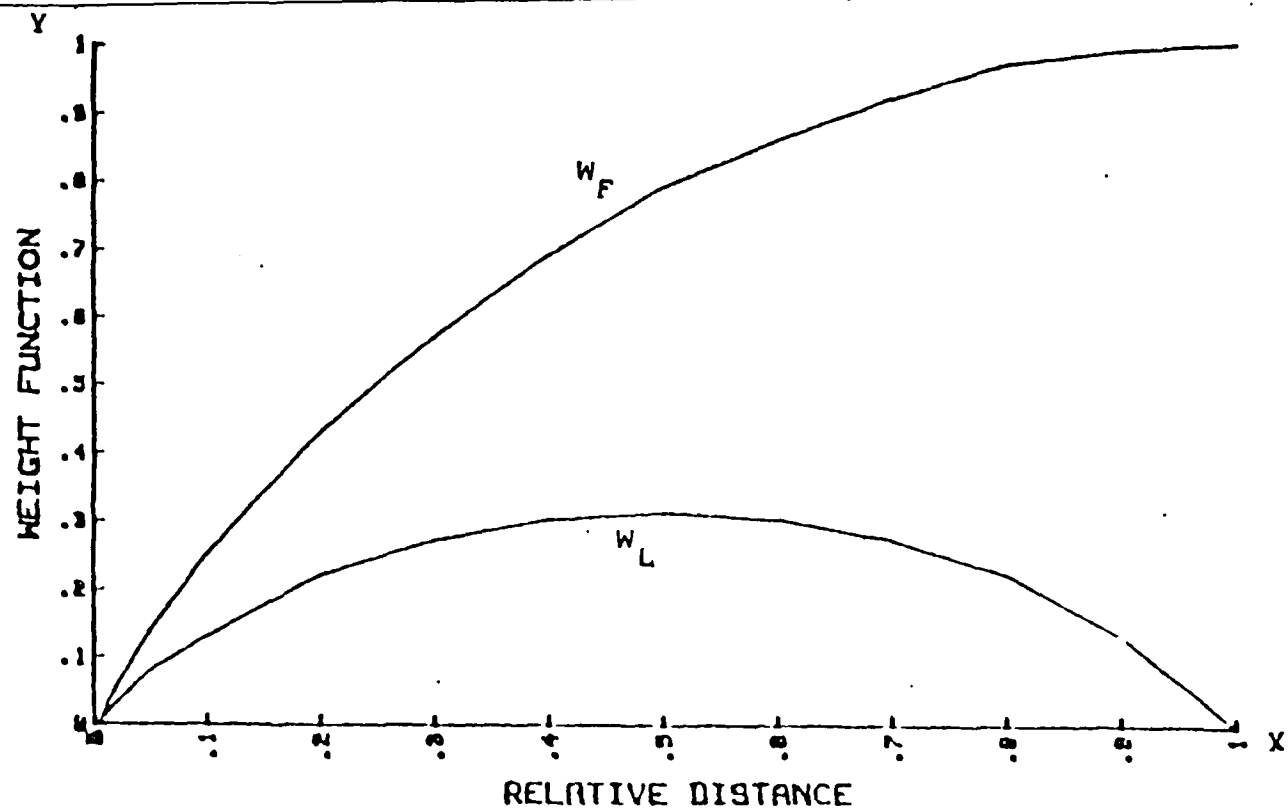

Figure 1.1 The Weighting Function of Spherical Waves in the cases of a single path (W_L) and a folded path with $\theta = 0$ (W_F). X represents the relative location along the path. For single path ; the source at $x = 0$ and the detector at $x = 1$. For a folded path ; the source and the detector are at $x = 0$, the mirror is at $x = 1$.

(folded path), or,
distance between detector and source,
(direct path).

Figure 1.1 shows the two weighting functions. In our set-up, Zo was 61 meters for the path. From Figure 1.1, in the case of an exact folded path ($\theta = 0$), the main contribution to the scintillation comes in the vicinity of the mirror. In the case of the single path, the main contribution is from the center of the path.

Ze'evi further noted that it was unlikely that we could find the proper conditions under which $C_n^2(x)$ along an atmospheric path is constant. Speer, B. A. [Ref. 5] Costantine, A. G. [Ref. 7] Henry, L. M. [Ref. 8] had already undertaken to test the Ze'evi prediction at NPS. Their results were inconsistant but did indicate that Ze'evi's prediction was wrong. The main goal of this experiment was the utilization of a controlled environment turbulence chamber to test Ze'evi's predicted weighting function for scintillation along a folded path. We used a plane mirror, a corner cube, a cat's eye in the experiment and compared the resulting scintillation measurements with Ze'evi's predictions.

the reflectors were disturbed during the experiment. Throughout a run we attempted to vary the voltage applied to the heating coil to stabilize C_T^2 . The input power to the heater was varied from 44.5 to 110 watts but we failed to truly stabilize C_T^2 . As a result of this problem, we decided to normalize all data for C_T^2 changes.

The quiet tunnel scintillation was measured and used as a reference. Then the heater was turn on, and after warming up, we measured the scintillation data, C_T^2 and the internal temperature at the same time. The heater tunnel section was then moved to the next position. The procedure was repeated for each data point. The standard deviations computed by the DATA 6000 were used to calculate the log variance of the intensity fluctuations.

By subtracting each experiment's respective "quiet" tunnel variance from the individual position variance during actual runs we got the true effect of the turbulence at that position. These results were then plotted versus each path position, along with a least squares fit to compare Ze'evi's weighting fuction.

C. EXPERIMENTS

1. First Experiment(Corner Cube) ---- 11 Oct 1984

For the experiment, the equipment was set up as described in section II . We put a 60 pound lead brick in each tunnel section, five lead bricks on the laser source platform and five bricks on the reflector bench to prevent vibrations. The weather conditions were clear and the wind was calm. We maintained the power to the heat source at 44.5 watts. The velocity of air through in turbulence chamber was about 45 ft/min.

Because we almost got a slope of 2/3 for the logarithm of the structure function $D_T(r)$ versus a fuction of

the logarithm $|\bar{r}_\lambda - \bar{r}_i|$, we made our scintillation measurements with the turbulence chamber under these conditions.

The data were collected at nine heater positions, 8.42, 15.74, 23.06, 30.38, 37.70, 42.58, 47.46, 52.34, and 57.22 meters, measured from the detector end. Figure 3.1 shows the log intensity variance versus the distance of the turbulence from the detector for this experiment. The values are normalized and include a plot of Ze'evi's weighting with the results. Detailed data is listed in Appendix A. We can not explain the jump after the 42.58 meter position.

2. Second Experiment(Corner Cube)----12 Oct 1984

After analyzing the first experiment, we found that small disturbances of the reflector affected the measurement values. We made a hole just behind the panel of the detector and attached a vinyl sheet with a screen to watch the scintillation fluctuations. We retaped all of the tunnel sections to prevent unwanted wind drafts and decided to add the baffle to the turbulence source tunnel to isolate the turbulence source from the tunnel environment.

In this trial we sampled ten points along the path at 57.22, 52.34, 47.46 42.58, 37.70, 30.38, 23.06, 15.74, 8.42, and 1.1 meters. We observed the weighting at the reflector end to be suddenly higher. The plot of Ze'evi's weighting and the data are shown in Figure 3.2, with the complete results in Appendix B.

3. Third Experiment(Corner Cube)---17 Oct 1984

In reviewing the previous two trials. We had considerable difficulty in maintaining the signal strength throughout the experiment. The external weather was clear

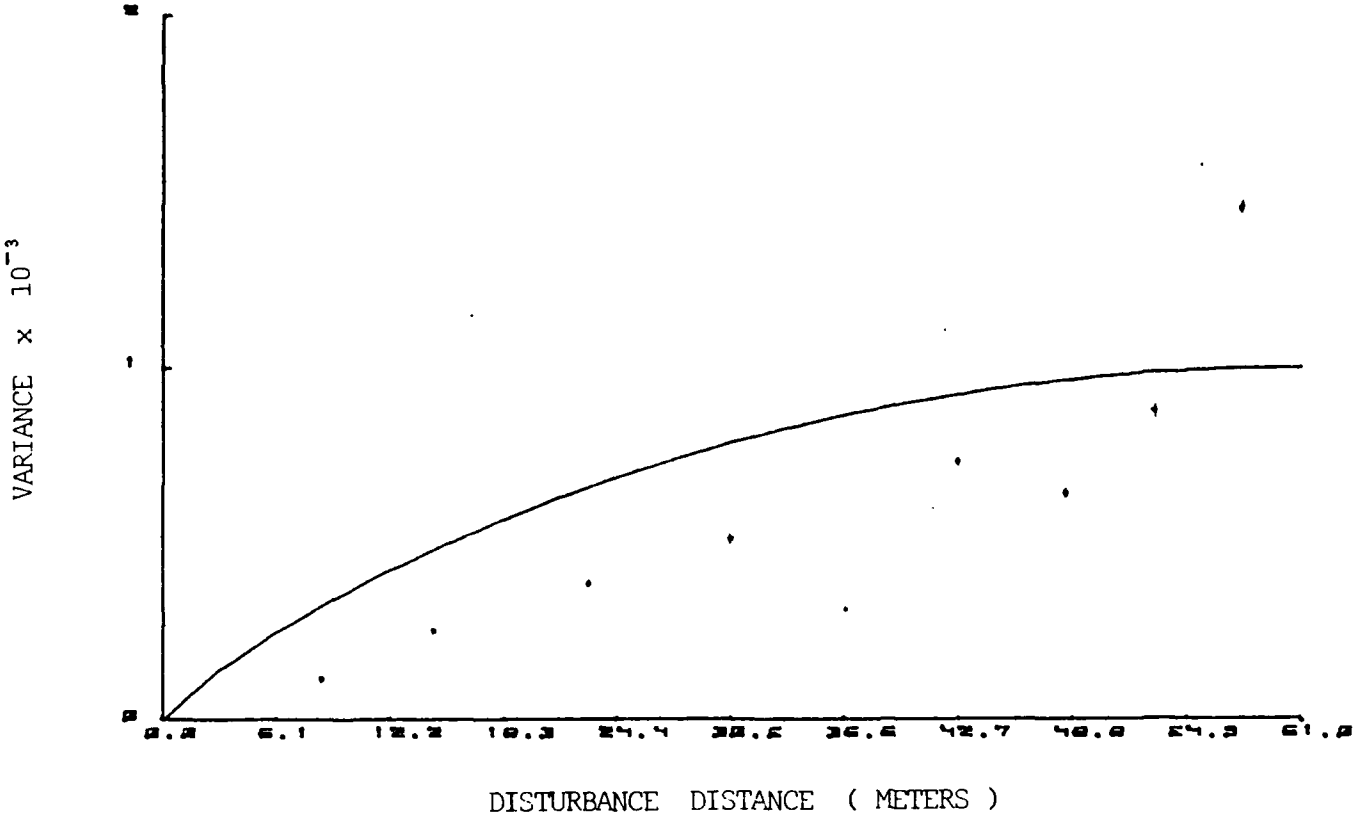

Figure 3.1 The Results of the First Experiment (Corner Cube). The solid line represents Ze'evi path weighting function.

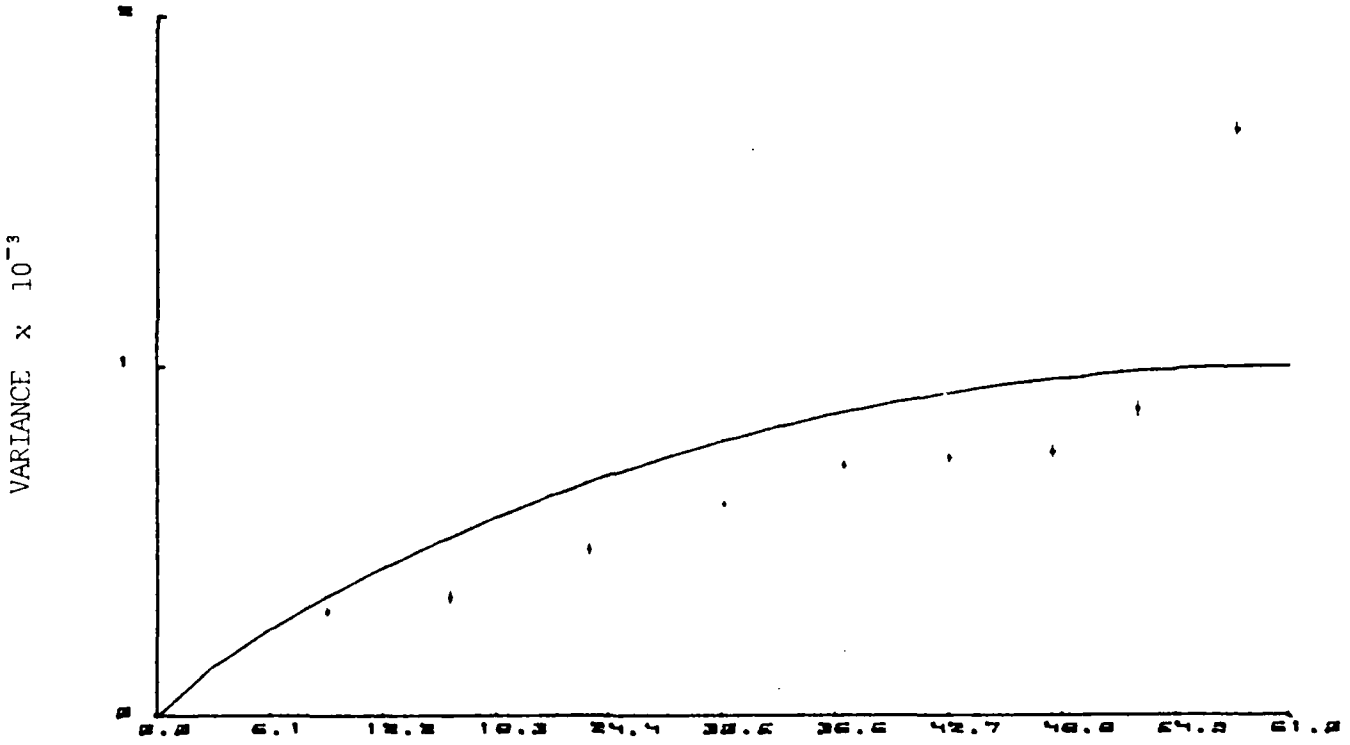

Figure 3.2 The Results of the Second Experiment (Corner Cube). The solid line represents Ze'evi path weighting function.

but the wind was appreciable. We retaped all of the tunnel sections. In this trial we selected ten path points, the same as in the second experiment. The results were not good. We suspected that the external wind conditions influenced the results. The plot is shown in Figure 3.3 with detailed results in Appendix C.

4. Fourth Experiment(Flat Mirror)---20 Oct 1984

For this trial, we set up the flat mirror instead of the corner cube. The D.C. power supply of the detector and the gain of the amplifier were the same as for the corner cube. The external weather was cloudy and the wind was calm. After this run, we found that the D.C. power supply of the detector decreased from 250 volts to 210 volts altering the gain. Since the variance of the log intensity is independent of the mean intensity a slow change in the detector bias voltage would not affect the results. In the analysis of this experiment, the data trend was completly different from Ze'evi's predictions. The plot showed that, the pattern was not weighted enough near the detector to about the 30 meter position and increased abruptly near the reflector. The plot of variance versus disturbance location from the detector are presented in Figure 3.4. Detailed results are in Appendix D.

5. Fifth Experiment(Flat Mirror)----22 Oct 1984

We rearranged all of the devices, laser source, chopper, convex lens, detector and reflector and rechecked the data reduction equipment. We did not find anything unusual. The pattern of this run was similar to the fourth experiment. A large increase occured at the end near the

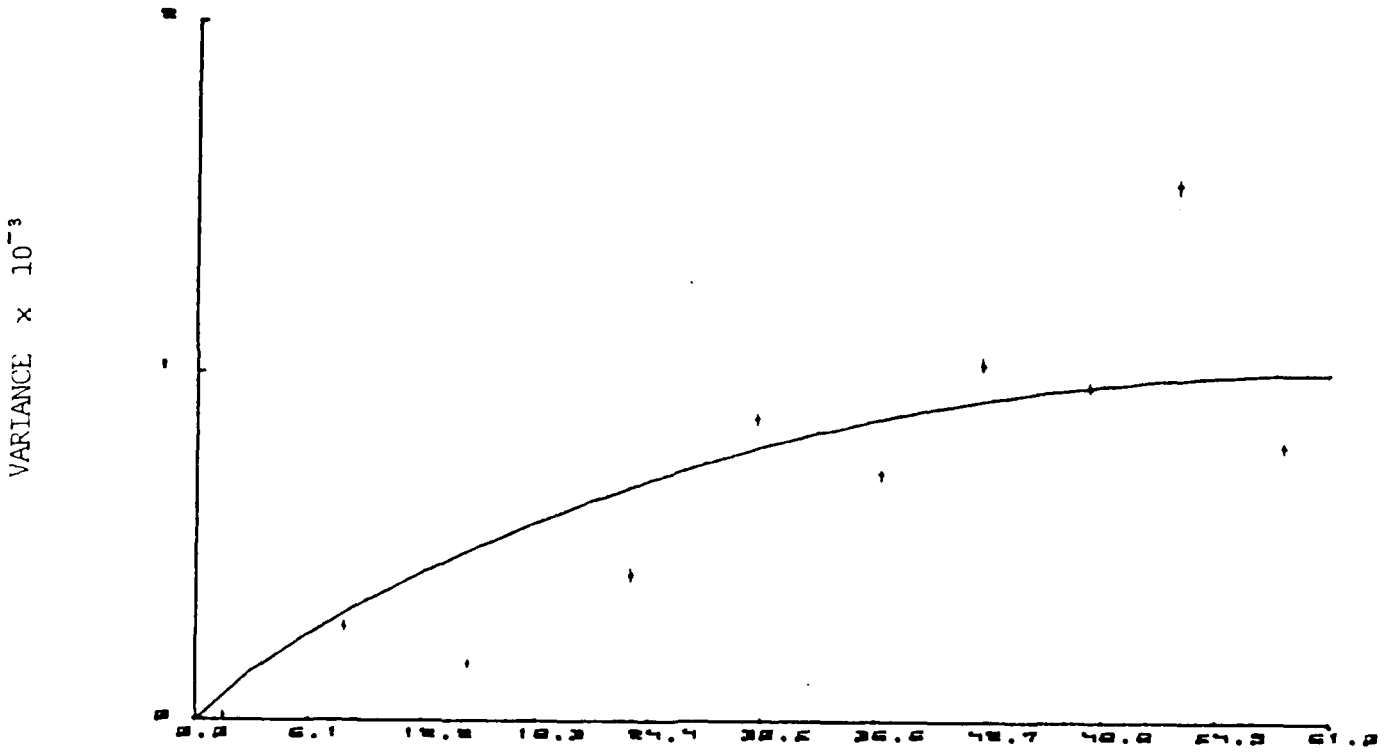

Figure 3.3 The Results of the Third Experiment (Corner Cube). The solid line represents Ze'evi path weighting function.

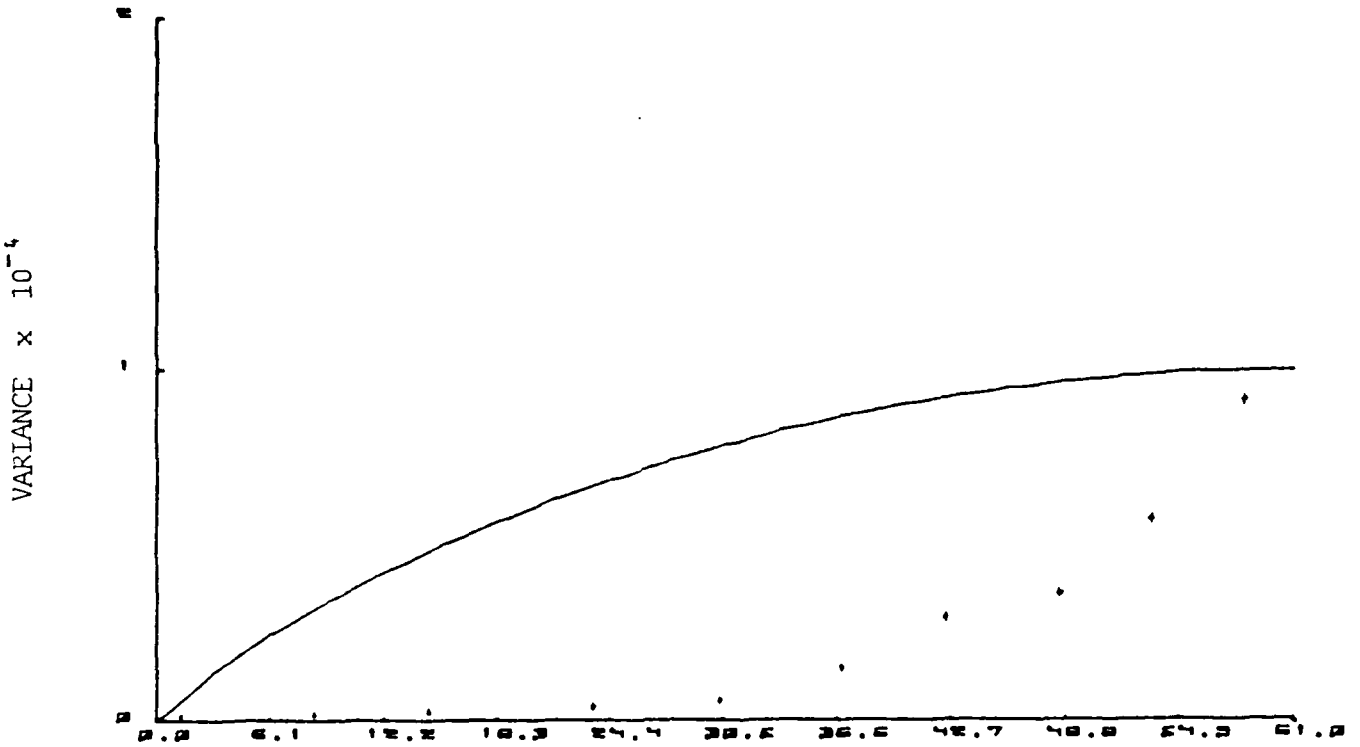

Figure 3.4 The Results of the Fourth Experiment (Flat Mirror). The solid line represents Ze'evi path weighting function.

reflector. The results are shown in Figure 3.5, with detailed results in Appendix E.

6. Sixth Experiment(Flat Mirror)---24 Oct 1984

We suspected that our heater was not drawing air in smoothly from the outside. In order to creat a positive flow of air upward through the beam and out the tunnel chimney, we fixed a wooden plate on both sides of the heater in the tunnel opening and all of the tunnel section was closed tightly.

The last 57.22 meter position had less weight than the 53.22 meter position. The total pattern followed the two previous experiments. The plot is shown in Figure 3.6 with detailed results in Appendix F.

7. Seventh Experiment (Cat's Eye)---2 Nov 1984

We spent a lot of time aligning the cat's eye. But we failed to get an exact alignment, because we found that the folded path beam on the screen was distorted. The intensity of scintillation was too weak so, we took out the convex-lens. After that, We observed the interference pattern of the splitter, which may have been due to disturbing the platform of the laser source during the movement of the heat source. After alignment of the laser source, we restarted from the 15.74 meter position.

The results we obtained follow the general pattern of Ze'evi's prediction, but it showed a pattern of less weight in all positions. The plot of variance versus disturbance location from the detector is presented in Figure 3.7. Detailed statistcs are located in Appendix G

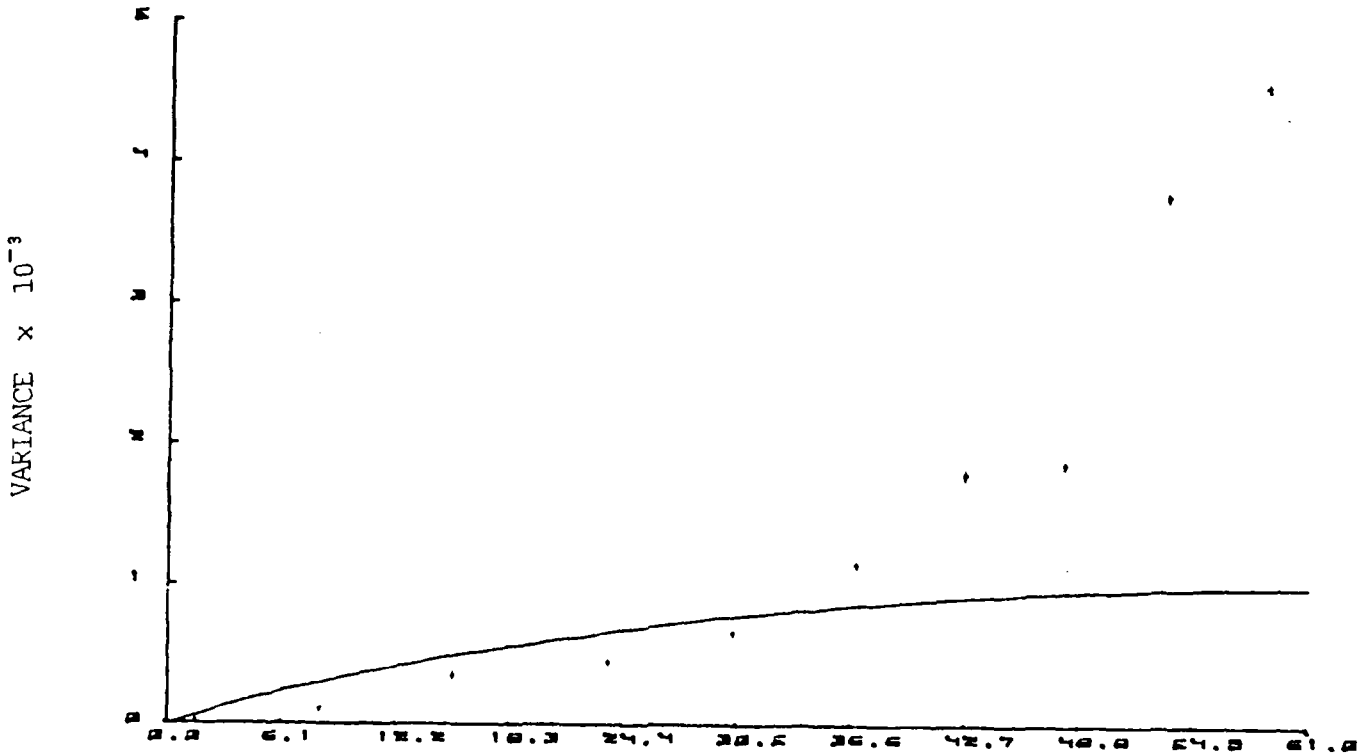

Figure 3.5 The Results of the Fifth Experiment (Flat Mirror). The solid line represents Ze'evi path weighting function.

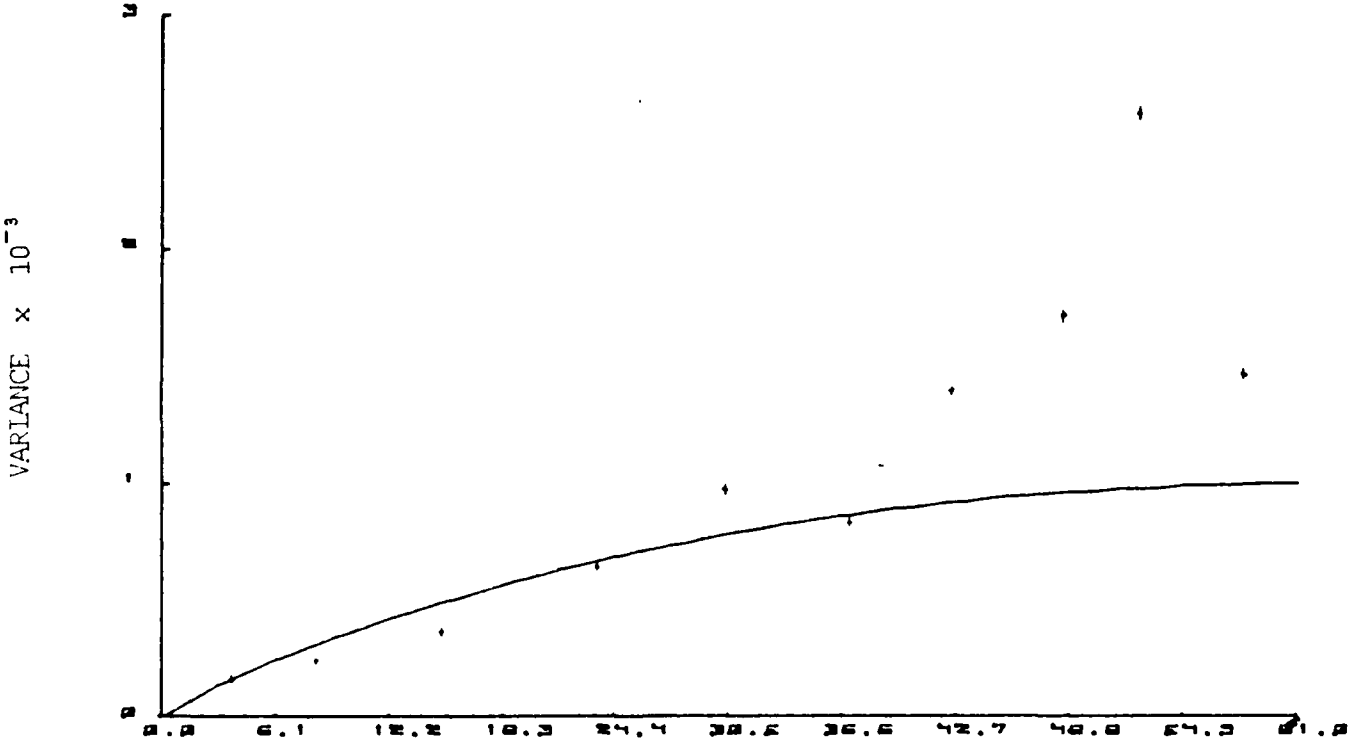

Figure 3.6 The Results of the Sixth Experiment (Flat Mirror). The solid line represents Ze'evi path weighting function.

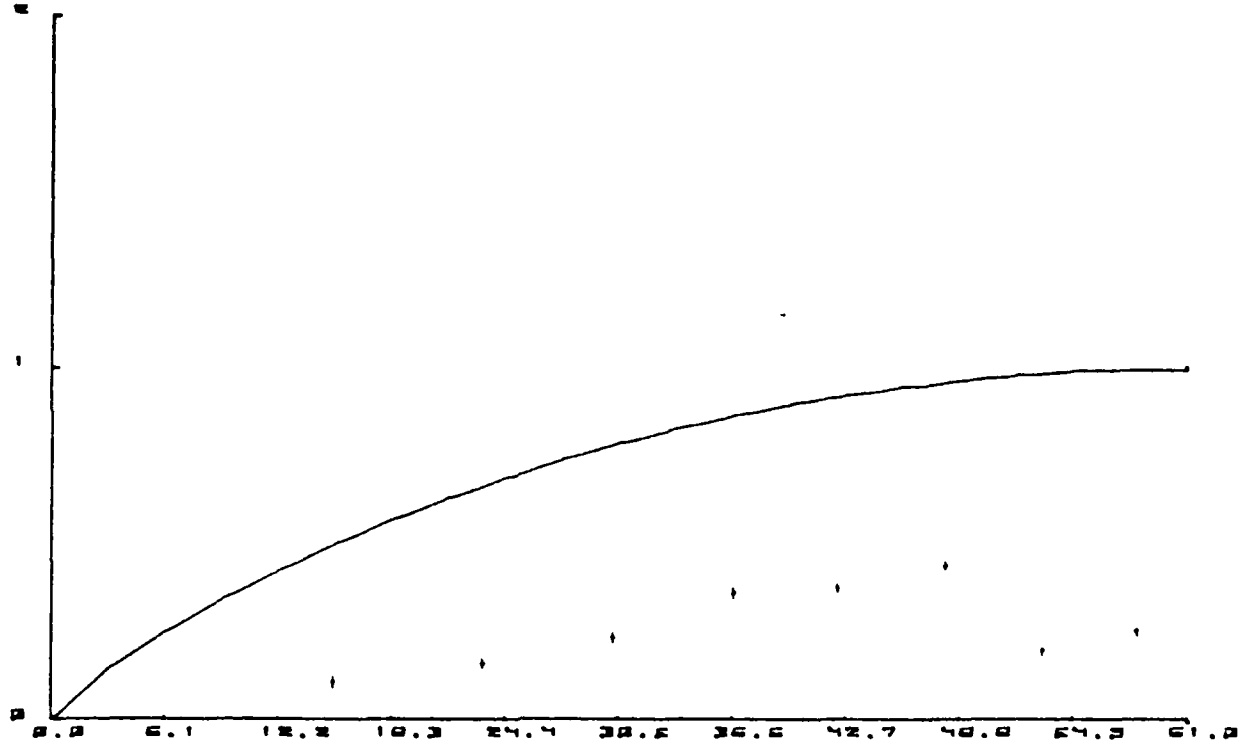

Figure 3.7 The Results of the Seventh Experiment (Cat's Eye). The solid line represents Ze'evi path weighting function.

8. Eighth Experiment(Cat's Eye)---4 Nov 1984

We tried aligning the cat's eye again. But the pattern of the curve was still distorted. We collected data in reverse starting from the reflector end. The results were nearly the same as the seventh experiment. The plot is shown in Figure 3.8, with detailed result in Appendix H.

9. Ninth Experiment (Cat's Eye)---12 Nov 1984

We changed all of the batteries and increased the power of the heat source to the 110 watts. From the start to about 30 meter position, the pattern of the curve followed Ze'evi's prediction. At the end of the target the pattern suddenly dropped. The plot of variance versus disturbance location from the detector is presented in Figure 3.9. Detailed statistics are located in Appendix I

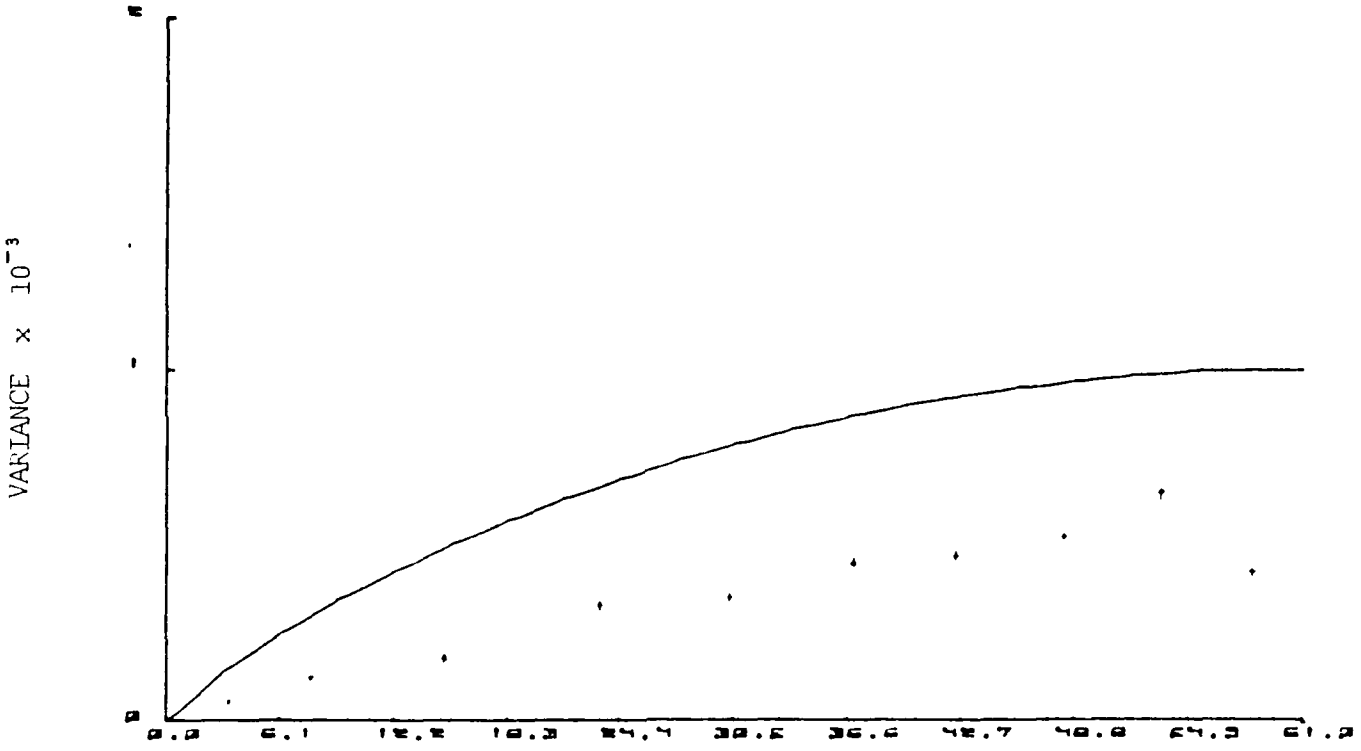

Figure 3.8 The Results of the Eighth Experiment (Cat's Eye). The solid line represents Ze'evi path weighting function.

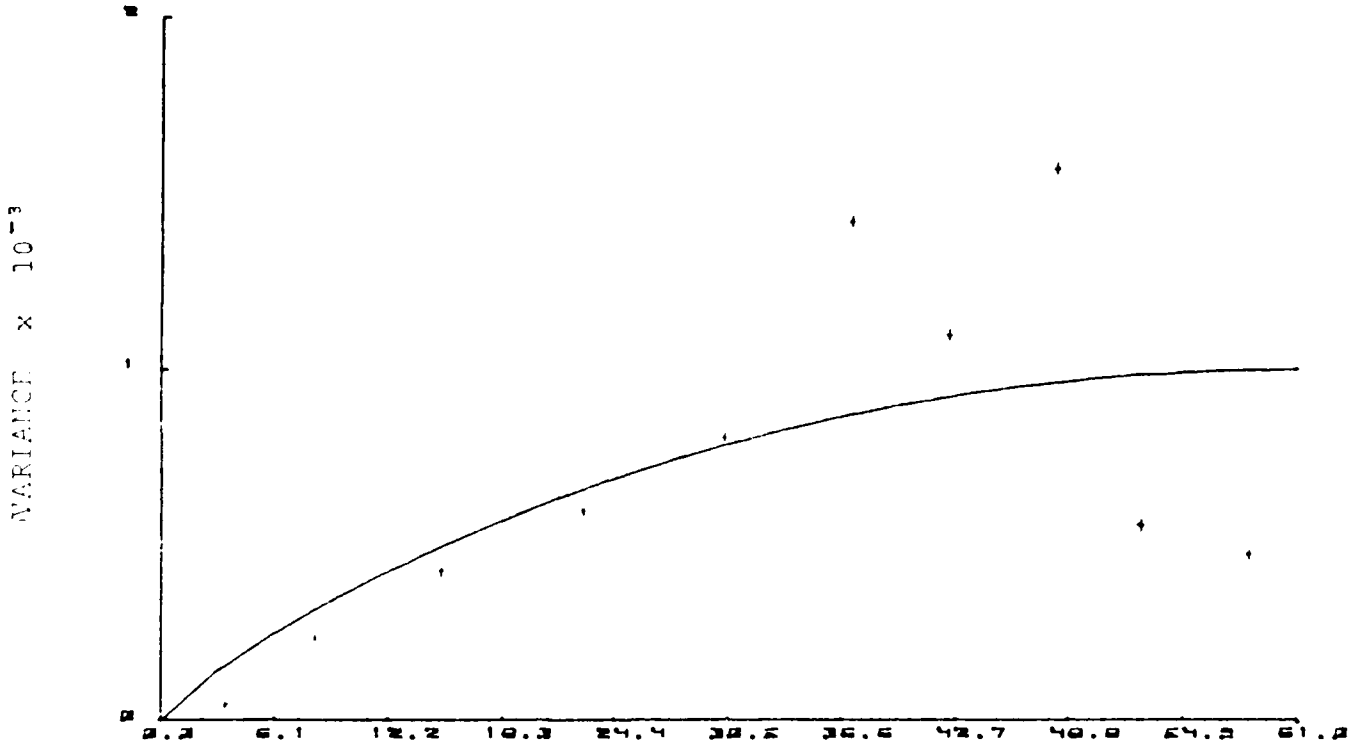

Figure 3.9 The Results of the Ninth Experiment (Cat's Eye). The solid line represents Ze'evi path weighting function.

THE DATA OF THE NINTH EXPERIMENT (CAT'S EYE) - 11. NOV. 1984

Disturbance Distance (Meters)	$\langle\sigma_i\rangle$	$(\langle\sigma_i\rangle^2-\langle\sigma_{quiet}\rangle^2)\times10^{-2}$	$C_T^2(K^2/m^{-2/3})$	$(\langle\sigma_i\rangle^2-\langle\sigma_{quiet}\rangle^2)\times10^{-2}$ Normalized for C_T^2
Quiet	.0709 ± .0023			
3.55	.1250 ± .0029	1.062 ± .341	233.0	.4705 ± .152
8.42	.1709 ± .0055	2.420 ± .333	122.2	1.999 ± .151
15.74	.2341 ± .0223	4.996 ± .723	130.1	3.975 ± .323
23.06	.2899 ± .0010	7.831 ± .446	130.1	5.912 ± .199
30.38	.3029 ± .0026	8.672 ± .630	105.1	7.974 ± .282
37.70	.2993 ± .0091	8.089 ± .607	55.39	14.425 ± .272
42.58	.2596 ± .0119	6.243 ± .457	53.43	11.390 ± .204
47.46	.2501 ± .0148	5.763 ± .594	34.64	16.120 ± .267
52.34	.2072 ± .0031	3.796 ± .385	64.26	5.741 ± .172
57.22	.1803 ± .0099	2.758 ± .432	61.57	4.385 ± .193

THE DATA OF THE EIGHTH EXPERIMENT (CAT'S EYE) - 4. NOV. 1984

Disturbance Distance (Meters)	$\langle\sigma_i\rangle$	$(\langle\sigma_i^2\rangle-\langle\sigma_{quiet}\rangle^2)\times10^{-2}$	$C_T^2(K^2/m^{-2/3})$	$(\langle\sigma_i\rangle^2-\langle\sigma_{quiet}\rangle^2)\times10^{-2}$ Normalized for C_T^2
Quiet	.1564 ± .0029			
3.55	.1703 ± .0042	.4570 ± .1912	30.25	.6015 ± .0855
8.42	.1810 ± .0013	.8295 ± .0592	30.33	1.092 ± .0265
15.14	.2113 ± .0005	2.042 ± .0624	55.25	1.432 ± .0368
23.00	.2431 ± .0005	3.472 ± .4246	44.29	3.078 ± .1899
30.38	.2636 ± .0010	4.502 ± .1892	53.09	3.286 ± .0846
37.70	.2844 ± .0029	5.646 ± .2390	55.78	3.945 ± .1069
42.58	.2714 ± .0091	4.929 ± .4613	47.25	4.152 ± .2063
47.46	.2724 ± .0010	4.974 ± .1503	40.44	4.882 ± .0672
52.34	.2543 ± .0003	4.030 ± .5677	24.80	6.498 ± .2539
57.22	.1956 ± .0083	1.383 ± .2528	12.96	4.248 ± .1130

THE DATA OF THE SEVENTH EXPERIMENT (CAT'S EYE) - 2. NOV.1984

Disturbance Distance (Meters)	$\langle\sigma_i\rangle$	$(\langle\sigma_i\rangle^2-\langle\sigma_{quiet}\rangle^2)\times10^{-2}$	$C_T^2(K^2/m^{-2/3})$	$(\langle\sigma_i\rangle^2-\langle\sigma_{quiet}\rangle^2)\times10^{-2}$ Normalized for C_T^2
Quiet	.0779 ± .0003			
15.74	.1510 ± .0049	1.676 ± .0975	39.36	1,003 ± .0436
23.06	.1791 ± .0083	2.291 ± .2792	31,26	1,709 ± .1248
33.38	.2120 ± .0016	3.843 ± .1911	39.32	2.231 ± .0855
37.70	.2037 ± .0213	3.555 ± .5070	24,51	3,260 ± .2269
42.58	.1701 ± .0031	2.288 ± .1999	15.48	3,351 ± .0894
47.46	.1705 ± .0078	2.309 ± .3134	11.50	4.454 ± .1402
52.34	.1386 ± .0049	1.182 ± .1461	10.94	2.394 ± .0653
57.22	.1339 ± .0021	1.187 ± .1111	8.799	3,001 ± .0497

APPENDIX C

THE DATA OF THE SIXTH EXPERIMENT (FLAT MIRROR) -24. OCT. 1984

Disturbance Distance (Meters)	$\langle\sigma_i\rangle$	$(\langle\sigma_i\rangle^2-\langle\sigma_{quiet}\rangle^2)\times10^{-2}$	$C_T^2(K^2/m^{-2/3})$	$(\langle\sigma_i\rangle^2-\langle\sigma_{quiet}\rangle^2)\times10^{-2}$ Normalized for C_T^2
Quiet	.1675 ± .0005			
3.55	.1884 ± .0008	.7429 ± .0390	14.39	1.448 ± .0174
8.42	.2165 ± .0047	1.880 ± .1614	19.98	2.681 ± .0722
15.74	.2437 ± .0060	3.382 ± .2871	27.07	3.636 ± .1284
23.06	.2934 ± .0088	6.093 ± .3608	28.47	6.146 ± .1613
30.38	.3645 ± .0223	10.50 ± .1109	28.37	10.60 ± .4961
37.70	.4014 ± .0130	13.32 ± 1.345	46.95	8.224 ± .6015
42.58	.4178 ± .0062	14.66 ± 1.038	28.98	14.64 ± .4643
47.46	.4698 ± .0065	19.30 ± 1.987	30.77	18.18 ± .8886
52.34	.4788 ± .0080	20.14 ± 1.495	21.02	26.88 ± .6688
57.22	.4951 ± .0184	21.73 ± 1.666	39.93	15.27 ± .7451

THE DATA OF THE FIFTH EXPERIMENT (FLAT MIRROR) - 22. OCT. 1984

Disturbance Distance (Meters)	$\langle\sigma_i\rangle$	$(\langle\sigma_i\rangle^2-\langle\sigma_{quiet}\rangle^2)\times10^{-2}$	$C_T^2(K^2/m^{-2/3})$	$(\langle\sigma_i\rangle^2-\langle\sigma_{quiet}\rangle^2)\times10^{-2}$ Normalized for C_T^2
Quiet	.1868 ± .0013			
1.1	.1921 ± .0008	.2020 ± .0399	9.174	.6981 ± .0179
8.42	.2218 ± .0010	1.432 ± .1515	38.11	1.199 ± .0678
15.74	.2649 ± .0093	3.536 ± .4215	39.84	2.842 ± .1885
23.06	.3033 ± .0005	6.079 ± .3721	50.16	3.715 ± .1664
30.38	.3794 ± .0016	10.33 ± .5296	47.30	6.932 ± .2368
37.70	.4392 ± .0049	15.72 ± .3619	42.03	11.40 ± .1619
42.58	.4930 ± .0138	20.85 ± 2.071	33.48	19.28 ± .9262
47.46	.4445 ± .0023	16.28 ± 1.147	24.98	20.18 ± .5128
52.34	.4651 ± .0101	18.20 ± 1.789	14.34	38.69 ± .8003
57.22	.4540 ± .0070	17.15 ± 1.684	11.19	46.53 ± .7529

THE DATA OF THE FOURTH EXPERIMENT (FLAT MIRROR) - 20. OCT. 1984

Disturbance Distance (Meters)	$\langle\sigma_i\rangle$	$(\langle\sigma_i^2\rangle - \langle\sigma_{quiet}^2\rangle)\times10^{-2}$	$C_T^2 (K^2/m^{-2/3})$	$(\langle\sigma_i\rangle^2 - \langle\sigma_{quiet}^2\rangle)\times10^{-2}$ Normalized for C_T^2
Quiet	.1882 ± .0010			
1.1	.1907 ± .0005	.0966 ± .0243	14.37	.2375 ± .0108
8.42	.2141 ± .0005	1.045 ± .566	66.35	.5658 ± .0253
15.74	.2529 ± .0001	2.860 ± .4048	40.84	2.515 ± .1810
23.06	.2914 ± .0049	4.959 ± .5989	35.98	4.888 ± .2678
30.38	.3770 ± .0129	10.68 ± .9307	94.59	4.051 ± .4163
37.70	.4376 ± .0011	15.62 ±1.093	42.96	12.98 ± .4886
42.58	.4292 ± .0156	14.70 ± .9184	17.17	30.23 ± .4107
47.46	.4877 ± .0187	20.26 ±1.474	20.89	34.78 ± .6594
52.34	.5246 ± .0088	23.99 ±1.374	17.41	49.07 ± .6145
57.22	.4830 ± .0527	19.86 ±2.839	7.602	91.46 ±1.270

THE DATA OF THE THIRD EXPERIMENT (CORNER CUBE) - 17. OCT. 1984

Disturbance Distance (Meters)	$\langle\sigma_i\rangle$	$(\langle\sigma_i\rangle^2-\langle\sigma_{quiet}\rangle^2)\times10^{-2}$	$C_T^2(K^2/m^{-2/3})$	$(\langle\sigma_i\rangle^2-\langle\sigma_{quiet}\rangle^2)\times10^{-2}$ Normalized for C_T^2
Quiet	.0577 ± .00503			
1.1	.0607 ± .00221	.03386 ± .0209	9.658	.08787 ± .0093
8.42	.1267 ± .00026	1.278 ± .02517	12.51	2.535 ± .1148
15.74	.1840 ± .00571	3.059 ± .3619	57.86	1.319 ± .1618
23.06	.2390 ± .01038	5.379 ± .3249	41.37	3.200 ± .1453
30.38	.2668 ± .00259	6.787 ± .3605	19.61	8.385 ± .1612
37.70	.2763 ± .01063	7.403 ± .7506	27.03	6.569 ± .3357
42.58	.2276 ± .00233	4.846 ± .1269	10.90	10.603 ± .0563
47.46	.3290 ± .00700	10.50 ± .6285	25.37	9.810 ± .2811
52.34	.2747 ± .00156	7.213 ± .2585	10.55	16.10 ± .1156
57.22	.3141 ± .01582	9.551 ± .9293	28.08	7.997 ± .4156

THE DATA OF THE SECOND EXPERIMENT (CORNER CUBE) - 12. OCT. 1984

Disturbance Distance (Meters)	$\langle\sigma_i\rangle$	$(\langle\sigma_i^2\rangle - \langle\sigma_{quiet}^2\rangle)\times10^{-2}$	$C_T^2 (K^2/m^{-2/3})$	$(\langle\sigma_i\rangle^2 - \langle\sigma_{quiet}^2\rangle)\times10^{-2}$ Normalized for C_T^2
Quiet	.0477 ± .00023			
1.1	.0629 ± .00206	.1688 ± .017	20.74	.3546 ± .00078
8.42	.1245 ± .02194	1.332 ± .270	24.25	2.407 ± .1209
15.74	.1841 ± .00248	3.168 ± .291	52.52	2.624 ± .1299
23.06	.2278 ± .00739	4.972 ± .461	58.54	3.663 ± .2062
30.38	.2954 ± .01489	8.506 ± .485	67.69	5.446 ± .2170
37.70	.2737 ± .00930	7.273 ± .507	48.99	6.503 ± .2288
42.58	.2954 ± .00046	8.501 ± .355	52.19	7.165 ± .1586
47.46	.3014 ± .00826	8.863 ± .522	53.24	7.343 ± .2334
52.34	.3005 ± .01008	8.817 ± .838	44.03	8.933 ± .3735
57.22	.2576 ± .01455	6.426 ± .735	15.97	17.77 ± .3287

THE DATA OF THE FIRST EXPERIMENT (CORNER CUBE) - 11. OCT. 1984

Disturbance Distance (Meters)	$\langle\sigma_i\rangle$	$(\langle\sigma_i^2\rangle-\langle\sigma\rangle_{quiet}^2)\times10^{-2}$	$C_T^2(K^2/m^{-2/3})$	$(\langle\sigma_i\rangle^2-\langle\sigma_i\rangle_{quiet}^2)\times10^{-2}$ Normalized for C_T^2
Quiet	.1227 ± .0039			
8.42	.1298 ± .0013	.7085 ± .1288	25.41	1.106 ± .0576
15.74	.1820 ± .0015	1.808 ± .1155	33.51	2.176 ± .0516
23.06	.2011 ± .0060	2.542 ± .2282	31.91	3.205 ± .1020
30.38	.2434 ± .0034	4.424 ± .3191	38.77	4.558 ± .1427
37.70	.2721 ± .0019	5.899 ± .1894	81.73	2.863 ± .0847
42.58	.2901 ± .0071	6.910 ± .3029	38.22	7.054 ± .1354
47.46	.3363 ± .0062	9.803 ± .3388	61.03	5.925 ± .1515
52.34	.2885 ± .0019	6.835 ± .9150	28.54	8.797 ± .4092
57.22	.2296 ± .0073	3.766 ± .2777	9.772	15.16 ± .1242

baffle arrangement and external weather conditions. Since we have not met all of the requirements of the Ze'evi theory, we can not state firmly whether or not it is correct for which case. It is not correct for the flat mirror.

4. Recommendations

First, without disturbing the laser source, reflector and detector the measurements of scintillation should be continued in more detail.

Second, the turbulence chamber and heater should be modified in order to provide a source of turbulence consistent with theory.

Third, our results are nearly the same as Costantine and Henry's, so a study of Ze'evi theory needs to be performed.

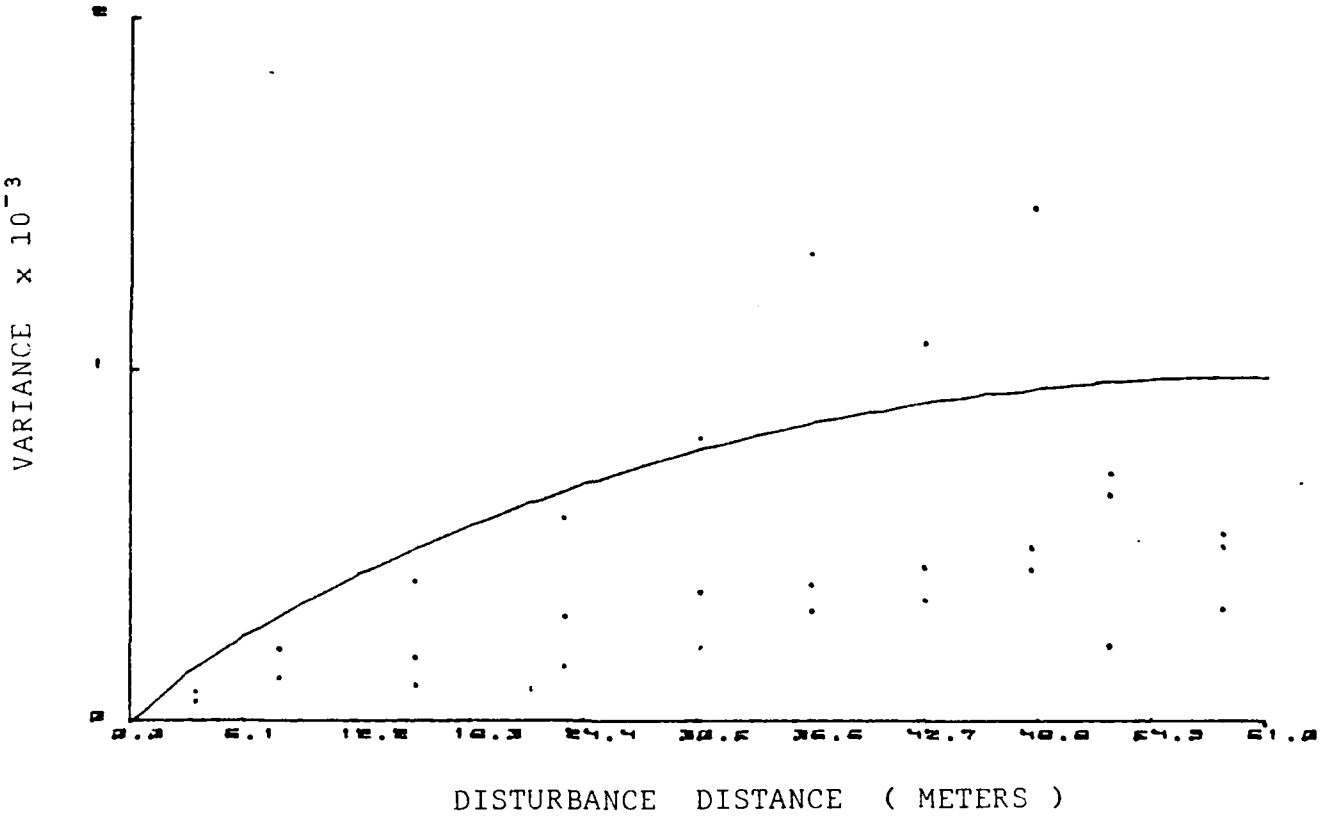

Figure 4.3 Cumulative plot of Cat's eye Data.

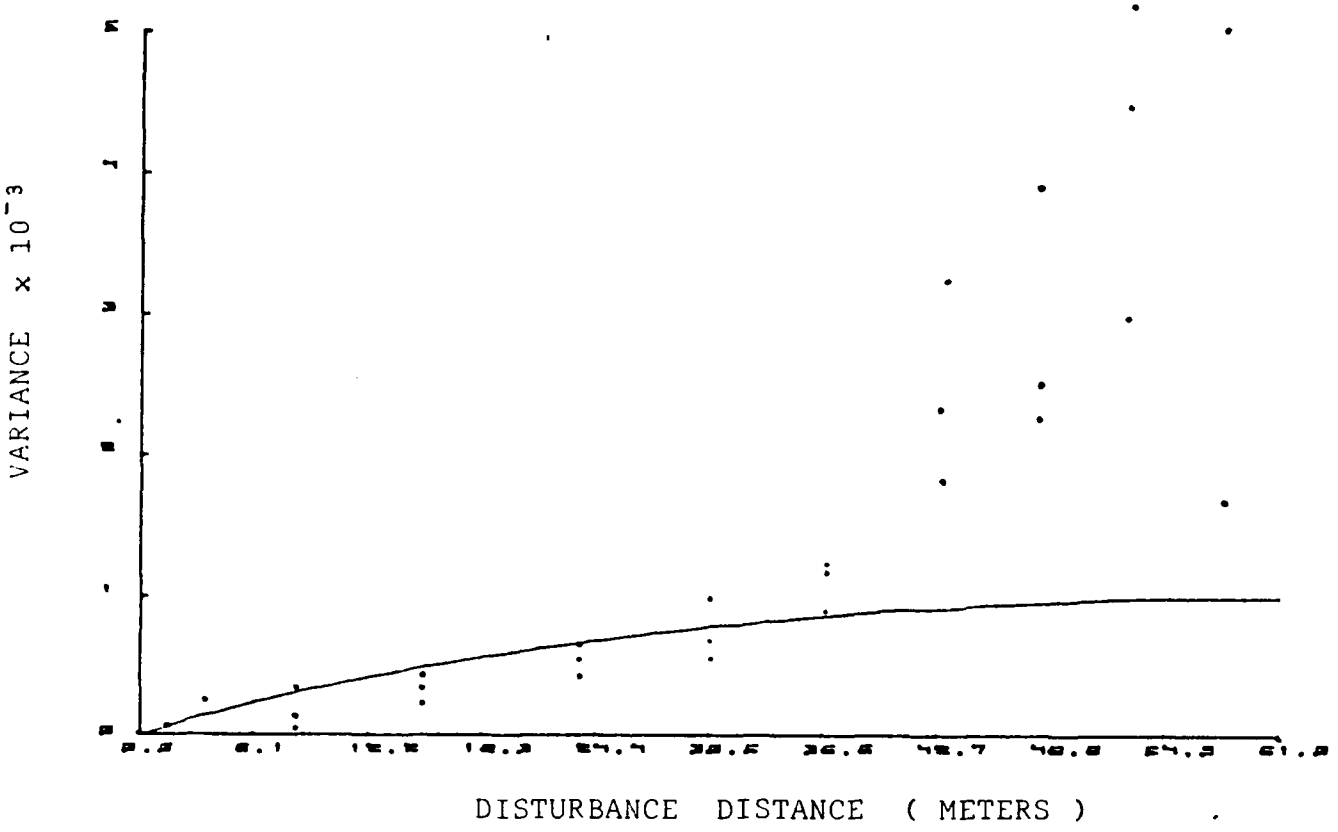

Figure 4.2 Cumulative plot of Flat mirror Data.

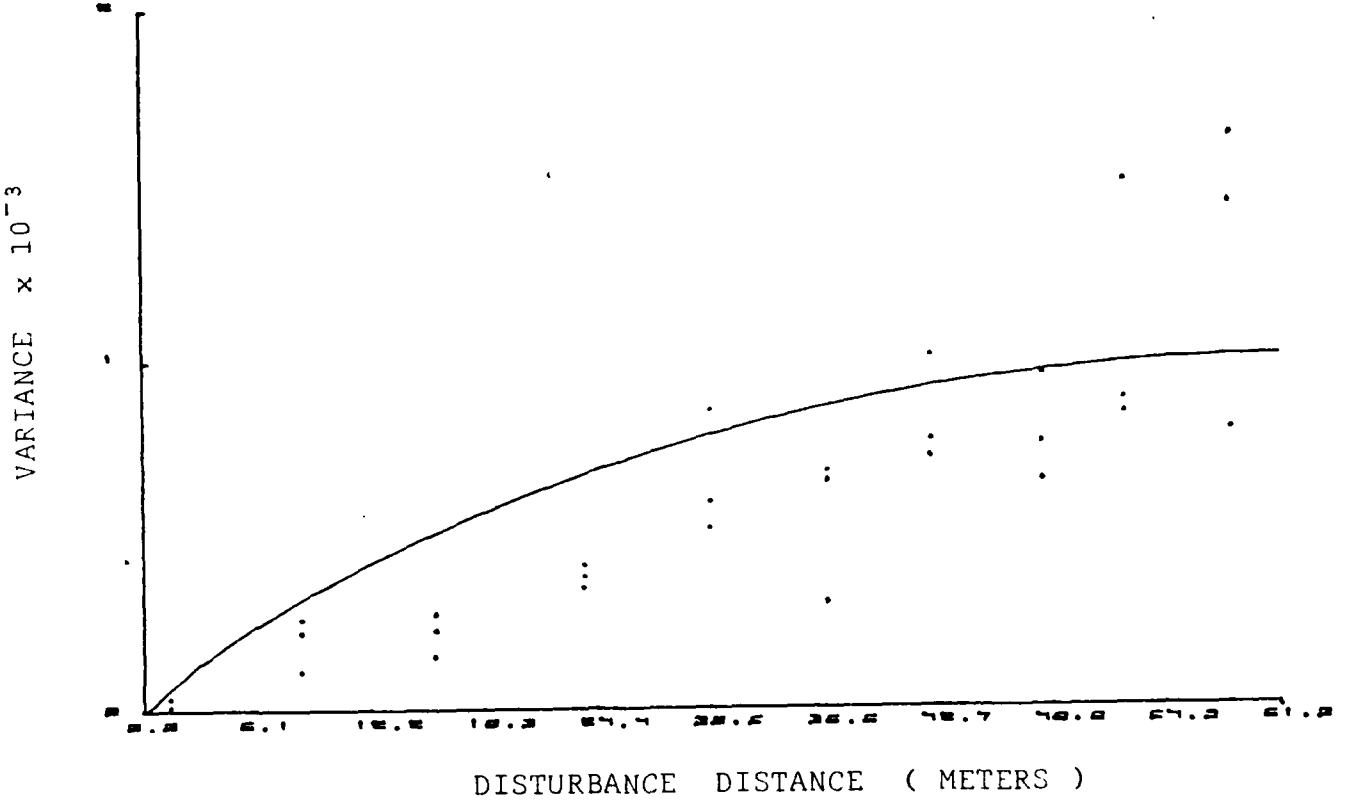

Figure 4.1 Cumulative plot of Corner Cube Data.

IV. RESULTS AND CONCLUSIONS

Based upon our experimental results and data analysis we find the following :

1. In examining our nine experimental runs we conclude that the data follows the general pattern of Ze'evi's prediction but fails to conform exactly to his predicted path weighting. The figures show a lower path weighting in the vicinity of the detector and a higher path weighting in the end of the target mirror.
2. The detailed results of each of the three reflectors are as follows. The corner cube tends to follow Ze'evi's general predicted form. But we got a higher path weighting in the vicinity of the target mirror. The Figure 4-1 shows the cumulative plots of all data for the corner cube. The flat mirror does not tend to follow the Ze'evi's predicted form at all. Our data indicate a low path weighting from the laser source to the 30.38 meter position. After this 30.38 meter position the path weighting inceases rapidly. Figure 4-2 shows the cumulative plots of all data for the flat mirror.

   The cat's eye tends to follow the pattern of Ze'evi's predicted form closely. But the values at all positions have less weight when the power of the heat source was 44.5 watts. Figure 4-3 shows the cumulative plots of all data for the cat's eye.

3. We conducted numerous trials with this measuring equipment, for various combinations of heaters, fans,

APPENDIX J

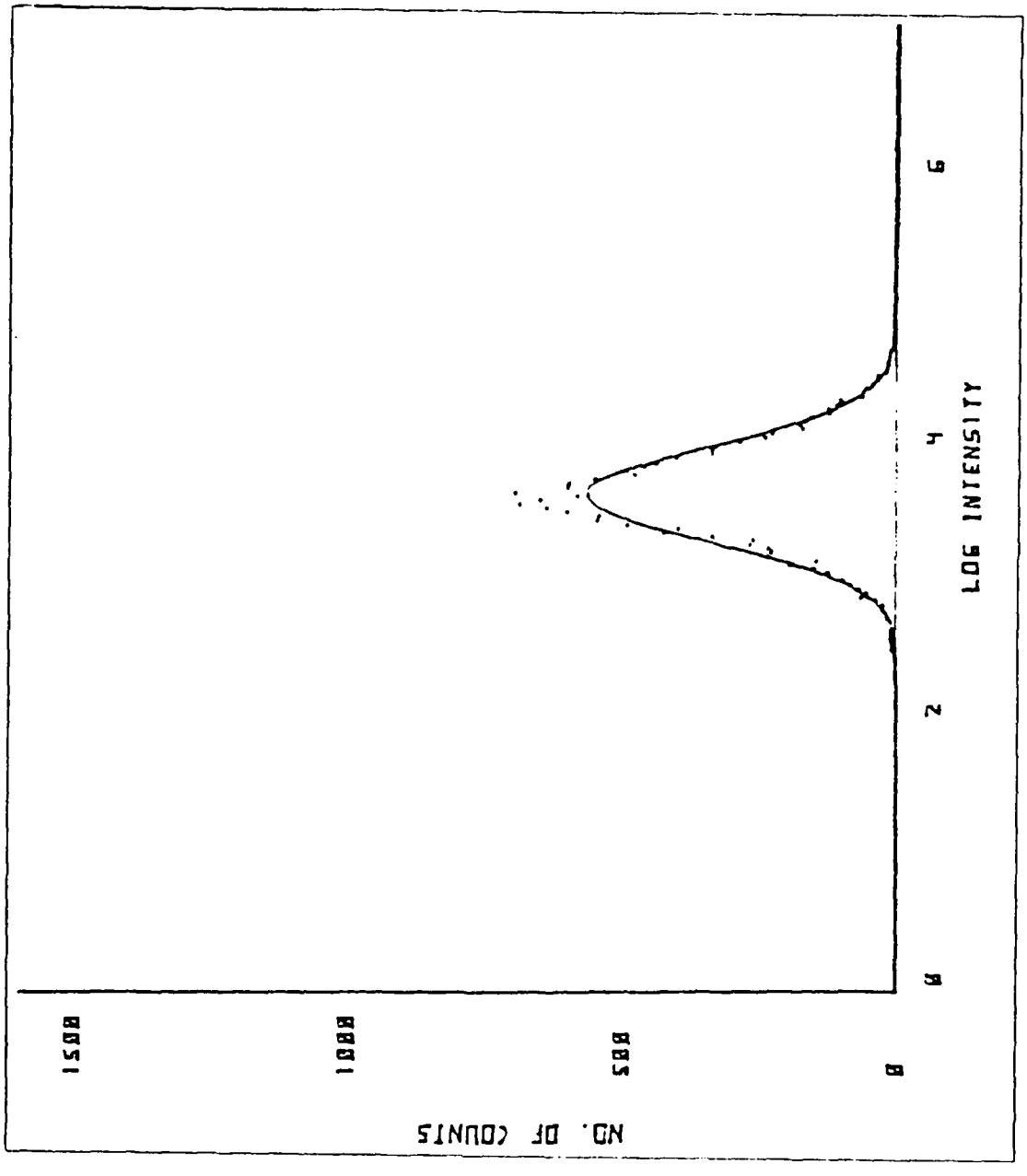

Figure J.1 Sample Scintillation Data and Theoretical Curve.

APPENDIX K

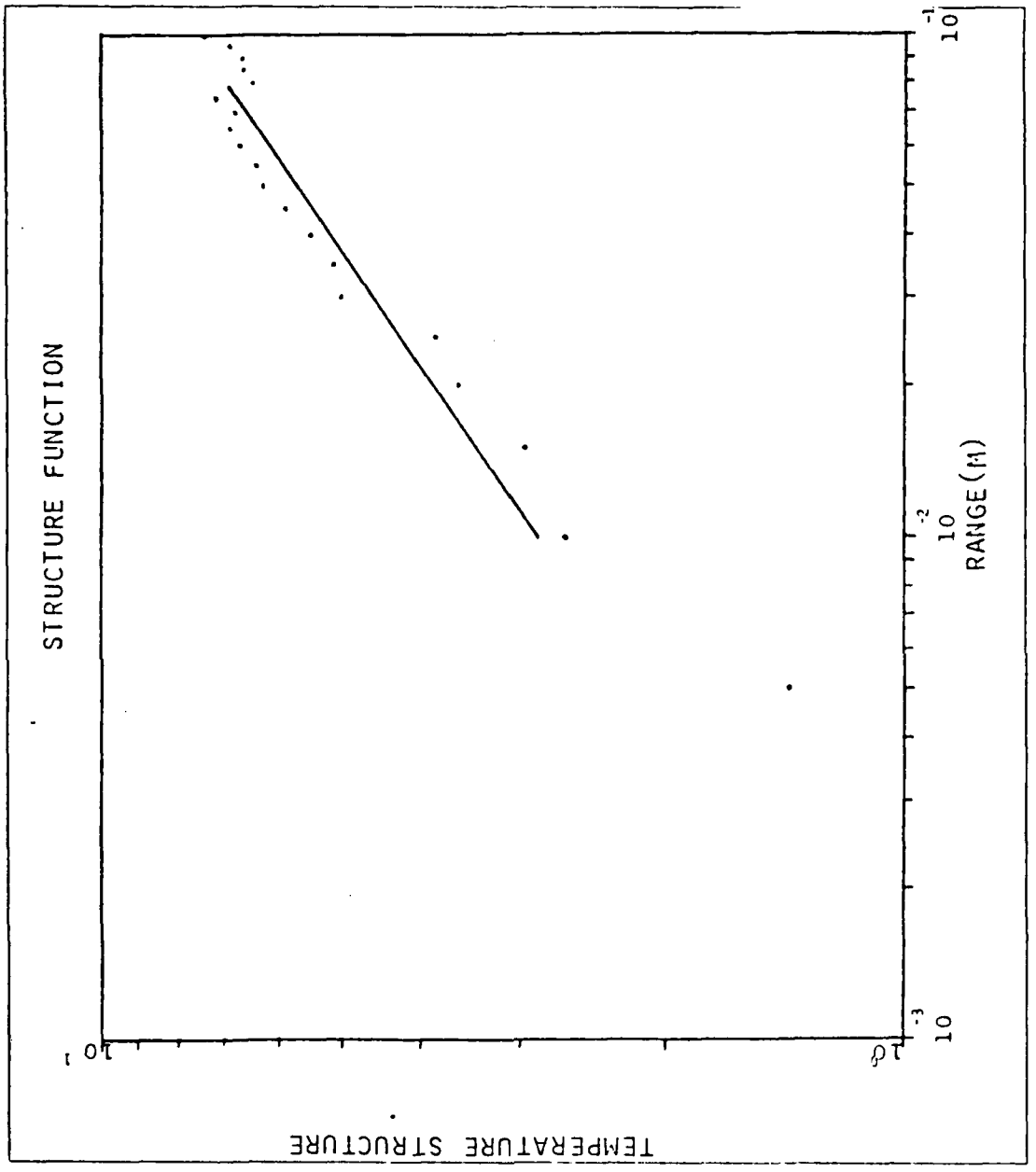

Figure K.1 Sample D_T Data and Theoretical Curve.

LIST OF REFERENCES

1. Tatarski, V. I., "The Effects of the Turbulent Atmosphere on Wave Propagation" Keter Press Binding , Isral, 1971.

2. Fried, D. L., "Propagation of a Spherical wave in a Turbulent Medium", JOSA, V.57, P.175, 1967.

3. Lutomisrski, R.F., and Yura, H.T., "Propagation of a Fninite Optical Beam in an Inhomogeneous Medium," Applied Optics, V.10, P.1652,1971.

4. Ze'evi, Avihu , Optical Scintillation along Folded Paths, PhD.Thesis, Naval Postgraduate School, Monterey, California, March 1982.

5. Speer, B. A.,and Parker, F. H., Measurements of Direct Path and Folded Path Optical Scintillation , M.S.THesis, Naval Postgradate School, Monterey, California, December 1982

6. Flenniken, R. J., Weighting for the Modulation Transfer Function, M.S. Thesis, Naval Postgraduate School, Monterey, California, June 1983.

7. Costantine, A. G., Measurements of Direct Path and Folded Path Optical Scintillation path Weightings, M.S. Thesis, Naval Postgraduate School, Monterey, California, June 1983

8. Henry, L. M., Measuremens of Direct Path and Folded Path Optical Scintillation Using a Corner cube Reflector, M.S. Thesis, Naval Postgraduate School, Monterey, California, December 1983.

9. Lee, J. B., Characterization the Tubulence in the Turbulence Section", M.S. thesis, Naval Postgraduate School, Monterey, California, December 1984.

10. Clifford, D. L., Ochs, G. R., Lawrence, R. S., "Saturation of Optical Scintillation by Strong Turbulence", JOSA V. 64, P. 148, 1984.

INITIAL DISTRIBUTION LIST

No.		Copies
1.	Library, Code 0142 Naval Postgraduate School Monterey, California 93943	2
2.	Department Chairman, Code 54 Department of Physics Naval Postgraduate School Monterey, California 93943	1
3.	Professor E.A. Milne, Code 61 Mn Dept. of Physics Naval Postgraduate School Monterey, California 93943	2
4.	Professor D.L. Walters, Code 61 We Dept. of Physics Naval Postgraduate School Monterey, California 93943	2
5.	Office of the Naval Attache Embassy of the Republic of Korea 2320 Massachusetts Avenue, Northwest Washington,D.C. 20008	1
6.	Library Officer Korea Naval Academy Chin hae, Kyung Nam, Korea 602-00	2
7.	Library Officer Seoul National University Kwan ak-Ku, Seoul, Korea	1
8.	Jong Hwan Kim 306-12, 29 tong 8 ban Ssang moon-dong, Do bong-ku Seoul, Korea	5
9.	Department of Ordnance Naval Head Quarter sin kil 7-dong, Yoeng dung po-ku Seoul, Korea	2
10.	Department of Physics Korea Naval Academy Chin hae, KyungNam, Korea	1
11.	San Ok Kim 88-1, Dea sa-dong, Dea jun-si Chung nam, Korea	2
12.	Defence Technical Information Center Cameron Station Alexandria, California 22314	2

END

FILMED

6-85

DTIC